

Hectospec, the MMT's 300 Optical Fiber-Fed Spectrograph

Daniel Fabricant, Robert Fata, John Roll, Edward Hertz, Nelson Caldwell, Thomas Gauron, John Geary, Brian McLeod, Andrew Szentgyorgyi, Joseph Zajac, Michael Kurtz, Jack Barberis, Henry Bergner, Warren Brown, Maureen Conroy, Roger Eng, Margaret Geller, Richard Goddard, Mike Honsa, Mark Mueller, Douglas Mink, Mark Ordway, Susan Tokarz, Deborah Woods, William Wyatt

Smithsonian Astrophysical Observatory, a member of the Harvard-Smithsonian Center for Astrophysics, Cambridge, MA 02138

`dfabricant@cfa.harvard.edu`

Harland Epps

Lick Observatory, UC Santa Cruz, Santa Cruz, CA 95064

and

Ian Dell'Antonio

Brown University, Box 1843, Providence, RI 02912

Received _____; accepted _____

ABSTRACT

The Hectospec is a 300 optical fiber fed spectrograph commissioned at the MMT in the spring of 2004. In the configuration pioneered by the *Autofib* instrument at the AAT, Hectospec’s fiber probes are arranged in a radial, “fisherman on the pond” geometry and held in position with small magnets. A pair of high-speed six-axis robots move the 300 fiber buttons between observing configurations within ~ 300 s and to an accuracy of ~ 25 μm . The optical fibers run for 26 m between the MMT’s focal surface and the bench spectrograph operating at $R \sim 1000\text{--}2000$. Another high dispersion bench spectrograph offering $R \sim 35,000$, Hectochelle, is also available. The system throughput, including all losses in the telescope optics, fibers, and spectrograph peaks at $\sim 10\%$ at the grating blaze in $1''$ FWHM seeing. Correcting for aperture losses at the $1.5''$ diameter fiber entrance aperture, the system throughput peaks at $\sim 17\%$, close to our prediction of 20%. Hectospec has proven to be a workhorse instrument at the MMT. Hectospec and Hectochelle together were scheduled for 1/3 of the available nights since its commissioning. Hectospec has returned $\sim 60,000$ reduced spectra for 16 scientific programs during its first year of operation.

Subject headings: instrumentation: spectrographs, techniques: spectroscopic, methods: data analysis

1. Introduction

1.1. Hectospec Overview

The Hectospec is a powerful fiber-fed spectrograph at the MMT Observatory in routine operation since April 2004. During its first year of operation, Hectospec obtained 60,000 spectra during 79 scheduled nights, with 48 nights of clear weather. Hectochelle, Hectospec’s high dispersion partner spectrograph, was scheduled for an additional 31 nights. In total, Hectospec and Hectochelle were scheduled for 1/3 of the available MMT nights. During Hectospec’s first year, it served 16 scientific programs.

Fabricant, Hertz & Szentgyorgyi (1994) and Fabricant et al. (1998b) outline the basic design of the Hectospec fiber positioner, its bench spectrograph, and optical fiber probes. Here, we emphasize: (1) the design refinements that occurred between 1998 and Hectospec’s delivery to the telescope in August 2003 and (2) Hectospec’s performance at the telescope.

1.2. The Converted MMT and Its Optics

The MMT’s f/5 optical system is comprised of a 6.5 m primary mirror, a 1.7 m secondary mirror, a series of large telescope baffles, a large refractive corrector, and a wave front sensor used periodically to correct the figure of the primary mirror and the telescope collimation. Fabricant et al. (2004) contains an overview of these components. Fata & Fabricant (1994) and Callahan et al. (2004) describe the f/5 secondary and its support. Fata & Fabricant (1993) and Fata, Krادينov & Fabricant (2004) discuss the f/5 wide field corrector in more detail. Pickering, West & Fabricant (2004) describe the Shack-Hartmann f/5 wave front sensor.

The wide field corrector has two modes of operation. For wide field spectroscopy with

optical fibers, the corrector provides a 1° diameter field of view on a curved but telecentric focal surface 0.6 meters in diameter. The sag of the spectroscopic focal surface is 8 mm. In the imaging mode, the corrector provides a field of view 0.58° in diameter on a flat focal surface. The spectroscopic mode of the corrector includes counterrotating atmospheric dispersion compensation prisms that are removed for the imaging mode.

The commissioning of Hectospec required the prior installation of the 1.7 meter f/5 secondary mirror at the MMT, which took place in April 2003. The wide field corrector and the f/5 wave front sensor were commissioned during May and June 2003. The first commissioning run with Hectospec took place in October 2003, and during this run we obtained observations of nearby galaxy clusters. The second Hectospec commissioning run was scheduled for April 2004. In mid April 2004 Hectospec was placed into routine operation.

1.3. Hectochelle

Hectochelle uses Hectospec’s robotic fiber positioner and optical fibers to feed a high dispersion bench spectrograph in place of Hectospec’s moderate dispersion spectrograph. Single orders, or several overlapping orders, dispersed by Hectochelle’s echelle grating are selected with bandpass filters. Szentgyorgyi et al. (1998) describe Hectochelle’s design.

2. Hectospec Fiber Positioner

2.1. Introduction

Hectospec’s robotic fiber positioner is unique for its high fiber placement speed while retaining high positioning accuracy. The high speed robots meet their design goals reliably:

150 paired moves of the tandem robots in under 300 seconds, and with 25 μm fiber positioning accuracy. The fiber robots attain this combination of high speed and accuracy due to a very stiff mechanical system that settles rapidly, powerful servo motors that rapidly accelerate the robots, and a sophisticated control system that incorporates many safety features while minimizing communication overhead between system components.

Hectospec’s fiber geometry was first used by *Autofib* (Parry & Gray 1986), an early robotic fiber-fed spectrograph for the Anglo-Australian Telescope with a single Cartesian robot positioning 64 optical fibers. Hectospec’s 300 fiber buttons are held onto the (400 series stainless) steel focal surface with NdFeB magnets mounted in the bottom of the fiber button. The magnets provide 200 g of holding force normal to the focal surface and >50 g of holding force in the plane of the focal surface.

2.2. Fiber Buttons and Focal Surface Assembly

Figure 1 shows a fiber button assembly from three angles. The 1.27 mm diameter stainless steel tube that protects the fiber after its exit from the fiber button is supported on its far end in brass pivot blocks. The fiber pivots are located 430 mm from the focal plane’s center. The pivots are arranged in two vertical levels so that the fiber syringes are fed into two vertical levels of separator trays. Using two levels provides more horizontal space in the separator trays and protects the syringes from excessive bending as the fiber button is moved tangentially on the focal surface. Figure 2 shows the (disassembled) fiber pivots outside the edge of the focal surface.

2.3. Mechanical Design

The fiber positioner can be separated into two parts to allow servicing of the robots and optical fibers. The upper unit (Figure 3) contains the two six axis robots and most of the electronics. The lower unit (Figure 4) contains the fiber probes, the fiber shelves (to prevent tangling of the optical fibers), the three guider probes and their track, the intensified camera for the guider probes, and the fiber derotator assembly that allows the fibers to follow instrument rotation. The two units are separated by removing protective covers and then unbolting the upper end of the struts that connect the two assemblies. Figure 5 is a top view of the assembled upper and lower units.

A pair of high-speed six-axis robots operating in tandem position Hectospec’s 300 optical fibers. Each robot forms a three-axis Cartesian (XYZ) system that carries a fiber gripper assembly. The Z-axis assembly (Figure 6) contains nested gimbals to allow placement of the fiber buttons perpendicular to the curved focal surface, as well as the gripper mechanism. Figure 7 shows the gripper assembly removed from the Z axis assembly. The Hectospec gripper design is based on the earlier Hydra design (Barden et al. 1993). Many mechanical details including parts lists are found in the Hectospec Hardware Reference Manual (<http://cfa-www.harvard.edu/mmti/hectospec.html>).

2.4. Speed and Accuracy

The timing budget for completing a Hectospec fiber repositioning consists of eight steps: (1) coordinated $XY\Theta\Phi$ motion to the next button position, (2) Z axis down, (3) gripper close, (4) Z axis up, (5) coordinated $XY\Theta\Phi$ motion to the new button position, (6) Z axis down, (7) gripper open, and (8) Z axis up. In total each fiber repositioning requires two coordinated $XY\Theta\Phi$ motions, four Z axis motions, and two gripper actuations. Table 1

gives approximate times for these motions; they total ~ 1.8 s.

A combination of factors set Hectospec’s internal positioning accuracy: (1) the accuracy of the servo loop closure, (2) the calibration of the axis encoders onto an orthogonal Cartesian coordinate system (includes axis home reference repeatability), (3) button movement as the gripper jaws are released, (4) the calibration of the fiber position within the button body, (5) flexure of the focal surface from zenith to the observing position, and (6) flexure in the guide probes over the course of an observation. Hectospec’s external positioning accuracy also includes contributions from astrometric errors for the targets and guide stars and instantaneous tracking errors. Table 2 summarizes the measured and estimated magnitudes of the internal positioning error sources. We set a goal of 0.025 mm for the total internal positioning error; Table 2 shows that the error contributions sum to 0.015 mm in quadrature and 0.036 mm in a worst case straight sum. The actual total internal positioning error lies in between these estimates, or about 0.025 mm.

2.5. Robot Safety Features

The fiber positioning system has multiple levels of safety features built into the hardware and the instrument control software. Our primary goal for these safety features is to prevent collisions between the robots, collisions of the robots with the focal surface or fibers on the focal surface, or high speed collisions of the robots into their mechanical limits of travel. Additional safety features act to minimize the resulting damage if a collision occurs. A large number of lower level safety checks stop robot motion on the detection of an error condition that could result in damage to some part of the instrument.

2.5.1. Collision Prevention

The pair of robots start each move segment simultaneously and they wait until both robots are finished before beginning the next move segment. (The eight move segments are listed in Section 2.4.) Error conditions from either robot stop both robots. During the paired moves the closest approach of the robots is 150 mm for the entire fiber pick and place operation. Limit switches that detect approaches of the robots closer than 150 mm or travel past the normal range of motion on all axes provide the next level of safety. Energy absorbing bumpers on the X and Y axes produce a controlled deceleration of the robots independent of the electronic and software systems once the limit switches are passed. The most difficult limit to detect is a downward movement of the Z axis, because the appropriate limit position varies over the focal surface due to its curvature. We built Z down limit switches into each of Hectospec’s three gripper jaws; these switches are activated if the jaws strike the focal surface or a fiber button. The entire gripper mechanism is spring loaded; the gripper mechanism retracts if the spring preload is exceeded.

2.5.2. Lower Level Safety Features

A key safety feature built into most servo controllers, including the Delta Tau Programmable Multi Axis Controllers (PMACs) used for Hectospec, is provided by the following error monitor. The following error is defined as the instantaneous difference between the commanded and actual positions read back from the encoder. The PMAC servo controller can be programmed to begin a controlled deceleration when a preset following error is exceeded. Each of Hectospec’s servo axes is protected by a following error limit. The following error protects against servo runaway if an encoder signal is lost and can provide safe shutdown if an obstruction is encountered. The following error provides no protection for moves shorter than the preset following error. An additional level of

protection is provided for Hectospec’s powerful X and Y axes: the signals from rotary encoders on the motor shaft and linear encoders on the axes are continuously compared with custom code in the PMACs and the system is shut down if a small error is exceeded.

Other safety features include over-temperature sensing, a PMAC CPU watchdog timer, amplifier fault detection, move time out protection, and a dropped button sensor, all of which terminate motion upon error detection. Many levels of error checking are also built into Hectospec’s control software to prevent setting a fiber button down on top of another button, to prevent striking a fiber button or part of the positioner structure with the robots, or to move a fiber button beyond its safe travel limits.

2.6. Robot Calibration Techniques

The major portion of Hectospec’s calibration was carried out with a custom grid of dots etched into an 0.61 m diameter Astrosital disk by Max Levy Corp. This calibration disk is the same diameter as Hectospec’s focal surface and is pinned and screwed into three support blocks in the guide probe tracks when in use. The grid is illuminated with high frequency fluorescent lamps carried on the robots, and the dot positions are recorded by the intensified cameras carried in the robot gripper assemblies. After averaging for 5 to 10 seconds, the noise in the dot position measurements is of order $2\ \mu\text{m}$. The dot positions have an intrinsic positional accuracy better than $6\ \mu\text{m}$. The positions of the dots recorded in the intensified robot cameras as the robots are commanded to move to the nominal dot position allows us to transform the XY encoder positions to an orthogonal Cartesian system. The largest errors prior to calibration are $\sim 40\ \mu\text{m}$, a testament to the accuracy of Hectospec’s machining and to the quality of the axis rails. Most of this error is due to: (1) small rotations of the robots as the gripper assembly moves along its rails and (2) the position of the encoders at the guide rails, 150 mm above the position of the fiber button in

the gripper jaws (and the position of the grid dots during calibration). The spacing of the guide blocks on the rails is also about 150 mm, so that deviations of the rail bed will map $\sim 1:1$ to deviations of the gripper jaws. This type of position sensing error is commonly termed Abbé error.

The gimbal axes were calibrated using the robot intensified cameras and a fine pattern of dots etched into a smaller grid placed on the focal surface. The Z axis scale is accurately determined by a rotary encoder and a precision ball screw driven through a 1:1 precision pulley system. A displacement measuring laser interferometer was used to verify that this scale is accurate to better than 1 μm RMS over the full range of travel. The ball screw accuracy is so high that we removed an unnecessary LVDT intended for Z axis feedback. (A small slip of $\sim 1 \mu\text{m}$ upon each downward movement of the Z-axis is removed by detecting a home sensor each time the Z-axis is raised.) The position of the focal surface relative to the robot axes was determined with a Kaman noncontact displacement probe mounted to the gripper assembly. The robots were commanded to move across the focal surface in a grid pattern, and the position of the focal surface was determined at each point.

2.7. Electronics

The main design challenge for Hectospec’s electronics was the distribution and routing of cables associated with the 15 motor axes and their associated encoders and limit switches. The weight and volume limits imposed by Hectospec’s Cassegrain mounting location precluded mounting the majority of Hectospec’s electronics onboard. The relatively large power supplies, servo amplifiers, stepper motor drivers, cable distribution boxes, and signal and power conditioning components are located in remote racks. A total of 20 cables with ~ 460 total conductors run between the fiber positioner and these racks, while 10 cables with ~ 110 total conductors run between the bench spectrograph and the electronics racks.

To maintain high reliability in the signal path, heavy-duty Mil-C circular connectors are used where cables must be disconnected to dismount the fiber positioner. The electronics rack contains seven main electronics boxes: (1) an interface box that accepts the Mil-C cables from the fiber positioner and distributes the signals to internal rack cables, (2) an interface box that performs similar functions for the bench spectrograph cables, (3) a signal conditioning and interface box for the Delta Tau PMAC servo controllers, (4) a pair of servo electronics boxes that contain the X,Y,Z, Θ , Φ servo amplifiers as well as the gripper stepper motor driver, (5) a stepper motor drive bay for the guider probe and spectrograph stepper motors, (6) a power supply box, and (7) a power conditioning and distribution module.

On the fiber positioner there are four electronics boxes: (1) the main interface box that accepts most of the Mil-C cables and distributes signals and power to internal cables, (2) a smaller interface box that accepts the Mil-C cables for the X,Y,Z servo motors, (3) an electronics box with a CPU and active circuits for on-board control functions, and (4) a small auxiliary box with an over-illumination sensor to protect the intensified cameras as well as power supplies for the fluorescent lamps used to illuminate the calibration grids.

Surge and over-voltage protection is provided in each of the main interface boxes at the fiber positioner, bench spectrograph, at the rack, as well as in the rack-mounted power conditioning box. Further details can be found in the Hectospec Hardware Reference Manual (<http://cfa-www.harvard.edu/mmti/hectospec.html>).

2.8. Guider Probes

The guider probes each move one section of a trifurcated coherent fiber bundle along an 86° arc just outside the focal surface plate that supports the fiber probes at the MMT focus. Fabricant et al. (1998b) describe the basic geometry of the guider probes. The guider

probes are actuated along a curved rail by a stepper motor driving a pinion gear against a large-diameter fixed gear. The guider probe has a brake mechanism, released by a solenoid, to hold the probe in place after the guider probe is positioned with the telescope zenith pointing. The largest challenge with this mechanism was designing a brake mechanism that would grip firmly and that could be released with the limited force available from the solenoid. Limited clearance from the structure precluded use of a large solenoid, and we reworked this mechanism twice to reduce the friction in the brake release mechanism. In future instruments pneumatic actuators might be a good replacement for solenoids because the pneumatic actuators offer a better power to weight ratio and do not dissipate as much heat.

2.9. Instrument Control Computers

The Hectospec fiber positioner is controlled by a Motorola 142 VME single board computer running Linux. This computer is mounted in the same VME rack that houses the two VME Delta Tau PMAC servo controllers. The **hctserv** server program running on the Motorola 142 accepts high and low level commands from clients and issues the appropriate motion control commands to the PMACs. Normally, the fiber positioner is operated by sending a high level sequence command to move the fibers from one configuration to another. The sequence begins when the client program reads the current fiber configuration from the **hctserv** server which is stored in static memory. The client computes the sequence of fiber pick and place operations required to go from the current to the new configuration, and prepares a sequence table of paired pick and place moves for the two robots. The sequence table is sent to the **hctserv** server, which checks that the sequence table can execute without crossing fibers or colliding the robots. Each paired move is successively loaded into the PMAC and executed.

A rack mounted Intel-based PC running Linux, “Snappy”, contains three Data Translation DT3155 frame grabber boards that capture images from the two robot TV guiders and the three guider probes. Snappy also communicates with the fiber positioner’s internal electronic box through an RS-232 interface to control the gain of the intensified TV guider cameras, to control internal lamps, and to monitor motor temperatures. A guider server running on a remote computer acquires guide frames from Snappy and calculates guide corrections for the telescope.

3. Hectospec Spectrograph

3.1. Mechanical Design

Fabricant et al. (1998b) describe the mechanical layout of Hectospec (see also Fabricant, Hertz & Szentgyorgyi (1994)) and Fata & Fabricant (1998) describe the optics mounts. Here we describe the dewar assembly and rotary shutter not previously discussed in the literature.

3.1.1. Dewar Design

Hectospec uses an internal focus catadioptric camera (Fabricant, Hertz & Szentgyorgyi (1994), Fabricant et al. (1998b)). Thus there is a premium upon minimizing the footprint of the CCD dewar support structure in the beam. The CCD dewar is an ~ 100 mm diameter cylinder supported on a thin vertical foot and by a thin-section horizontal evacuated tube that surrounds the dewar’s cold strap. The cold strap runs between the dewar and a liquid N_2 cryostat mounted outside the optical beam running to and from the on-axis camera mirror. The dewar window also serves as a field flattener lens for the camera. Figure 8 shows the dewar assembly. The dewar assembly is mounted on a focus stage.

3.1.2. Rotary Shutter

At the spectrograph entrance “slit”, the optical fibers are arranged in two parallel columns spaced ~ 1.6 mm apart. The fibers in each column are spaced on 0.96 mm centers, but the two columns are offset by 0.48 mm, giving a final effective fiber to fiber spacing of 0.48 mm. The width of the structure holding the fibers, the “fiber shoe”, has been minimized to reduce the obscuration of the beam returning past the fibers from the on-axis collimator mirror. A narrow rotary shutter assembly is mounted on the fiber shoe in front of the optical fibers. The rotating part of the shutter is an ~ 150 mm long slotted cylinder. The shutter is toggled between open and closed with 90° rotation actuated with a stepper motor. The rotary shutter assembly mounted on the fiber shoe is shown in Figure 9.

3.2. CCDs and Array Electronics

Hectospec uses two E2V model 42-90 4608X2048 CCDs with $13.5 \mu\text{m}$ pixels, arranged in a 4608X4096 array. The long axis of the CCDs are parallel to dispersion. Hectospec’s CCDs have superb cosmetic quality, and the entire two CCD array has only a single bad column. At a readout rate of $100,000 \text{ pixels s}^{-1}$, the readout noise is 2.8 e^- RMS. At the operating temperature of -120°C , the dark current is very low: 1 e^- in 900 s of integration. The electronics have a gain of $1 \text{ e}^- \text{ ADU}^{-1}$, matching to a few percent between the four amplifiers. The count rate due to background radiation is 1 event s^{-1} integrated over the region occupied by the fiber spectra on the two CCD array.

Hectospec shares its array controller electronics design with the other MMT f/5 optical and infrared instruments including Hectochelle, Megacam, and SWIRC. The design of these electronics was driven by the requirements of the 72 channel Megacam version (Geary 2000). Hectospec’s two CCDs are read out through four amplifiers in 46 sec.

3.3. Optics

3.3.1. Image Quality

Fabricant et al. (1998b) and Fabricant, Hertz & Szentgyorgyi (1994) describe Hectospec’s optics; here we describe the optical performance of the as-built spectrograph. Hectospec’s optics have a reduction of 3.45, with an anamorphic demagnification (in the spectral direction) of 1.06 with the 270 groove mm^{-1} grating. With perfect optics, the image of the 250 μm fiber should be an ellipse 5.4 by 5.1 pixels across. The RMS image diameters produced by the real optics, when illuminated by a point source emitting into an f/5.3 cone, are 1.3 to 1.8 pixels. Optical ray traces with ZEMAX predict that the azimuthally averaged two dimensional FWHM of the fiber image should be 4.8 to 5.0 pixels, which agrees with the observed azimuthally averaged FWHM. The tails of the observed images are broader than the ZEMAX prediction: the observed 95% encircled energy radius is 4.2 pixels compared with the predicted 3.5 pixels. We attribute this difference to small amounts of light emerging from the fibers at focal ratios faster than the modeled f/5.3; this light is imaged in the wings of the fiber image. We have a pupil mask at the grating to reject most of this focal ratio degraded light, but the mask is somewhat oversized to account for pupil rotation that depends on field angle.

We discovered one general feature of the HIRES style of camera (Epps & Vogt 1993) used in Hectospec: a ghost pupil is formed between the focal surface and the field flattener element by light reflected from the CCD and then back again from the front surface of the field flattener. The intensity of this ghost pupil is reduced by a factor of $\sim 10^{-3}$ relative to the main image and the ghost pupil area is nearly as large as the detector area. We noticed the ghost pupil because we operated the spectrograph briefly with a damaged antireflection coating on the front surface of the field flattener. The reflectivity of the damaged antireflection coating was about an order of magnitude larger than normal,

increasing the intensity of the ghost pupil by a corresponding factor. Once we replaced the field flattener with a undamaged spare, the ghost pupil faded into obscurity, but it may be wise to keep an eye on this issue in designs of this family of optics.

3.3.2. *Optical Coatings*

The initial optical coatings for the Hectospec spectrograph were developed for the FAST spectrograph (Fabricant et al. 1998a) at Whipple Observatory’s 1.5 m Tillinghast Telescope. FAST’s high throughput Sol-gel antireflection coatings and UV-enhanced overcoated silver reflection coatings gave many years of service and we expected the same performance in Hectospec. Hectospec’s Sol-gel antireflection coatings have been trouble free, but the first protected silver coatings on the Hectospec mirrors were noticeably discolored by late 2002, approximately three years after their coating. Reflectivity measurements indicated low reflectivity between 5000 and 6000 Å. We decided to strip the original coatings and to recoat with the Lawrence Livermore National Laboratory (LLNL) durable silver reflective coating (US Patent 6,078,425). The LLNL coating has slightly lower peak reflectivity than the original (fresh) coating, but offers much better reflectivity below 4000 Å.

3.4. Gratings

Hectospec’s 259 mm collimated beam diameter requires large custom ruled gratings. Hectospec currently has two gratings: a 270 groove mm^{-1} grating blazed at 5000 Å and a 600 groove mm^{-1} grating blazed at 6000 Å. In both cases we specified a 5000 Å blaze, but the blaze angle has proven to be the most difficult parameter to control in ruling these large gratings. The 6000 Å blaze for the 600 groove mm^{-1} grating was the closest to specification achieved in four attempts. The 270 groove mm^{-1} grating provides a dispersion

of $1.2 \text{ \AA pixel}^{-1}$ and a resolution of 6.2 \AA FWHM . The $600 \text{ groove mm}^{-1}$ grating provides a dispersion of $0.5 \text{ \AA pixel}^{-1}$ and a resolution of 2.6 \AA FWHM . Both gratings have a peak absolute efficiency of 72%. Higher ruling density gratings might be best provided by assembling grating mosaics.

4. Hectospec Optical Fibers

4.1. Design of Fiber Run from Positioner to Spectrograph

The design of the optical fiber run between the fiber positioner and bench spectrograph turned out to be a much larger challenge than we had imagined during the Hectospec’s conceptual design phase. Optical fibers offer a unique means of mapping a spectrograph slit efficiently onto a large number of objects distributed over a very large field of view. However, fibers must be used carefully if they are not to severely compromise the sensitivity of the spectrograph by degrading the focal ratio of the light incident on the fiber. Degradation of the focal ratio in a fiber results in a loss of light in the spectrograph optics unless the spectrograph optics are significantly oversized. Oversizing the optics is expensive in a spectrograph as large as Hectospec’s, and forming good images from the light scattered into faster focal ratios makes a difficult optical design problem harder. Focal ratio degradation arises from mechanical stress of the fibers. Focal ratio degradation will typically cause time variable throughput losses as the stress experienced by the fibers changes as the telescope pointing direction changes. These throughput variations are doubly troublesome because good sky subtraction relies on an accurate fiber to fiber throughput calibration.

We were aware from the time that we began work on Hectospec that the mounting details of the fibers in the fiber probes at the fiber positioner end and in the fiber slit at the spectrograph end of the fibers are important in controlling focal ratio degradation, but our

test program demonstrated the importance of what happens in between. We engineered thermal breaks in the teflon tubing to address the thermal expansion mismatch between the fused silica fiber and the teflon tubes that protect the fibers. Fabricant et al. (1998b) describe the basic design elements that we used to control focal ratio degradation in the fiber run. The other important design driver for the fiber run is that it must allow easy mounting and dismounting of the Hectospec on the telescope. Figure 10 shows the design of the fiber run and the position of the thermal breaks that allow for the differential thermal expansion of the fibers and their protective teflon tubes. Figure 11 is a closeup of one of the four thermal breaks in the fiber run.

4.2. Laboratory Tests of the Optical Fibers

Our specifications called for a total fiber throughput of 75% at 6000 Å into a focal ratio of f/5.3, the final focal ratio of the spectroscopic wide field corrector and the design focal ratio of the Hectospec bench spectrograph. At 6000 Å the internal absorption of Hectospec’s 26 m long fibers is 6%, the Fresnel reflection loss at the uncoated BSM51Y prisms at the fiber input end is 5.3%, and the Fresnel loss at the bare fiber output end is 3.5%. The total throughput accounting for only these three fiber losses is 86%, requiring that 87% of the light entering the fibers at f/5.3 exit within an f/5.3 cone if the total throughput specification is to be met. As Figure 12 shows, we met our goal for total fiber throughput with an average throughput of 77% and a standard deviation of 2%.

5. Observing with Hectospec

5.1. Observation Planning Software

Roll, Fabricant & McLeod (1998) describe the basic algorithms used in Hectospec observation planning to match fiber probes to targets. Currently, each Hectospec observer is responsible for planning the fiber configurations to be used at the telescope. The observer begins by assembling a catalog containing the desired targets as well as potential guide stars in the field. Observers may priority rank targets in the catalog and assign a minimum and maximum number of fibers to each rank. The guide stars and the targets must have excellent relative astrometry because the guide stars establish the field alignment. The observer uses the **xfitfibs** program to create instrument configuration files from the input catalog. **xfitfibs** combines the observation planning software with a graphical user interface (GUI). The observer may use **xfitfibs** to plan multiple fiber configurations with multiple field centers and to rank these centers in priority.

In addition to matching fibers to targets, **xfitfibs** selects guide stars, and assigns fibers for the measurement of the sky background. The user can drag field centers with a mouse or enter new field centers into a table and view the effects on a graphical display. The display indicates guide stars within range of the guide probes as well as those accessible by changing the instrument rotator angle. The **xfitfibs** software derives guide star magnitudes from either the 2MASS or GSC2 catalogs, removes stars outside the specified magnitude range, and additionally removes non-stellar objects using GSC2 classifications or by SExtractor classification from DSS images. Stars with close companions or brighter neighbors in the field of the guide probes are also excluded. Selection of bright guide stars ($R < 16$) minimizes setup time with the intensified robot and guide cameras and allows operation in the full moon.

5.2. Queue Operation

Hectospec is operated in queue mode to use valuable telescope time efficiently and to distribute the time lost due to weather, telescope and instrument malfunctions evenly. The goal of the queue scheduling is to distribute the available productive observing time proportionally to the nights scheduled by the Time Allocation Committees. The MMT is scheduled in trimesters, and the queue scheduling is for a single trimester at a time. The queue schedule must be continually updated through an observing run in response to the weather conditions and telescope/instrument performance. The observers provide the queue manager with completed fiber configurations, which include the sequence of observations, the fiber layout, and valid guide stars. These layouts are checked and then scheduled as time permits. The fiber positioner is operated by experienced robot operators on behalf of the queue. The robot operator also oversees the acquisition of calibration data in the late afternoon and early evening including HeNeAr wavelength calibrations, incandescent lamps for flatfielding, and typically twilight sky flatfield exposures. During the night, observers assigned telescope time operate the spectrograph and evaluate the data quality on behalf of the queue. Observers thereby gain firsthand experience with Hectospec’s operation and capabilities, avoiding some of the communication difficulties that others have reported in the operation of observing queues isolated from the scientist who will ultimately use the data.

5.3. User Interfaces

5.3.1. *Hobserve*

Hobserve (Figure 13) is a Tcl/Tk script that provides a step by step procedural interface that guides the robot operator through the procedure of calculating the appropriate

fiber configuration for the chosen observing time, calculating the sequence of fiber moves required to attain that configuration, issuing the move commands to the robots, and setting up the guiding on the field with the preselected guide stars. A separate graphical user interface (GUI) (**guidegui** (Figure 14) displays the guide star images superposed on the guider target positions. The **Hobserve** script coordinates the actions of several servers and calls other high level shell scripts to accomplish its functions.

5.3.2. *SPICE*

The **SPICE** Tcl/Tk program (Figure 15) provides a GUI interface to the spectrograph and camera controls and sequences the operations for various types of exposures. The GUI consists of two fixed displays at the top of the window along with several tab selectable displays that appear at the bottom of the window. The upper fixed display indicates the status of the system power controls and of the software servers that control hardware components. The text message within the status buttons and the color of the status buttons change together to indicate the instrument state. Toggling these buttons toggles the state of the power or software server. The lower fixed display provides housekeeping information as well as exposure status. The housekeeping items include the dewar temperature, the status of the calibration lamps, the tracking status of the ADC prisms, and the position of the wave front sensor carriage. The exposure status information includes the current exposure count within the requested number of exposures, the current exposure type (skyflat, object, bias, dark, etc.), and the current exposure state (exposing, reading out, etc.).

The observer can select one of four user-selectable tabbed displays: an initialization tool, a standard operations tool, a calibration lamp tool, and an observing log tool. The initialization tool controls the sequencing of powering up and homing the three spectrograph axes (shutter, focus, and grating stage), as well as bringing up the required software servers.

The standard operations tool is the main tabbed display window that the observer uses to acquire data and control the spectrograph. Within this window the grating rotation, focus position, and shutter status are displayed and can be controlled. The current fiber configuration file name is displayed, but the fiber configuration is controlled from the **Hobserve** interface. The observer selects the desired exposure type from a pull-down menu (object, dark, bias, domeflat, HeNeAr, focus, etc.) and specifies the desired exposure time and number of exposures. Pressing “Go” initiates the exposure sequence. During the initialization of the exposure, the software checks for possible problems including a mismatch between the requested and encoded grating rotation and focus position, blocking by the wavefront sensor, illumination of calibration lamps at inappropriate times, lack of guiding signals, and ADC prism tracking turned off. The focus procedure automatically moves the grating to the zero order position and takes a sequence of CCD charge-shifted exposures at different focus settings. The grating is returned to its nominal position at the end of the focus run. Focus changes during a run appear to be negligible.

The calibration lamp tool allows the observer to control the calibration lamps that illuminate a screen mounted on the MMT building shutters. The calibration lamps are mounted in four identical lamp boxes mounted in the MMT chamber. Lamp status, lamp voltages, and lamps currents are displayed in a comprehensive color-coded table.

The observing log tool provides a summary of each of the exposures in the selected night’s directory and a text box for the observer to annotate each exposure. A PostScript formatted observing log of all the exposures (with observer comments) for the current night is produced and archived.

5.4. Observing Sequence

At the beginning of the night or during an exposure on the previous field, the robot operator loads in the next fiber configuration in the “on-deck” window of **hobserve**. The expected start time and exposure duration of the observation are entered, and the fiber positions are retweaked for the airmass and instrument rotator position at the expected exposure midpoint. Depending on the nominal position angle entered during observation planning, the rotator demand angles may exceed the $\pm 90^\circ$ soft limits. Therefore, the position angle can be reset by the robot operator to minimize the rotator demand angles. If guide stars are available in two of the three guide star probes, the “on-deck” configuration is ready to go. If two guide stars are not available at this position angle, the position angle can be manually adjusted to find minimum rotator demand angles consistent with obtaining two guide stars. In the worst case, if two guide stars are not available at acceptable rotator angles, another configuration can be chosen without loss of observing time.

We begin the reconfiguration process by slewing the telescope to the zenith. The robots are capable of operating at any combination of zenith angle and rotator angle, but we reconfigure the fibers with the telescope zenith pointing to minimize the power dissipation and load on the drive components. After the robots reposition the fibers, the guide probes are moved to correct guide star positions. The telescope is then slewed to a bright star near the field position, and the wave front sensor is deployed to correct the primary support forces and telescope collimation. While the wave front sensor probe is retracted, the telescope is slewed to the field position and the instrument rotator is set to track the desired position angle. The robot guide cameras are sent to the guide star positions and the telescope pointing and the rotator angle are adjusted with autoguiding software until the guide stars appear at the positions corresponding to a fiber held in the gripper jaws. A pellicle beam splitter in the robot optical train allows 50% of the light to pass through to

the guide probes. The positions of the guide stars in the guide probes are captured and the guiding is then transferred to the guide probes. This procedure directly ties the guiding to the robot-defined coordinate system upon which the fibers are positioned. As soon as the robots are parked an observation can begin.

6. Hectospec Performance at the MMT

6.1. Throughput

We measured the throughput of Hectospec with the spectrophotometric standard star BD+284211, stepping the star across one of Hectospec’s fibers to determine the point of maximum throughput to eliminate light loss due to astrometric errors. With a direct spectrograph, the entrance aperture is normally opened as wide as possible to separate the measurement of spectrograph throughput from aperture losses. With fibers, the entrance aperture is fixed and we measure total throughput including aperture losses. Figure 16 shows the derived throughput measurement for BD+284211 in 1" FWHM seeing. We have separately calculated the aperture losses for Hectospec’s 1.5" diameter fibers as a function of seeing using images obtained with Megacam; in 1" FWHM seeing we find that a 1.5" diameter contains 59% of the light, giving an aperture correction of 1.7. Referring to Figure 16 and applying this correction, the system throughput peaks at $\sim 17\%$ between 5000 and 6000 Å. Our prediction for the total system throughput peaked at 20% in the same wavelength region, in reasonable agreement with the measurement.

6.2. Thermal Flexure of Bench Spectrograph

The room that encloses the Hectospec and Hectochelle bench spectrographs is one level above the telescope chamber floor, and shares a common wall with the telescope

chamber. The spectrograph room is not well insulated from the telescope chamber due to several doors and perforations. As a result, the temperature in the spectrograph room fluctuates considerably more than we had planned. The nightly temperature swings lead to temperature gradients in the optical bench and optical mounts that lead to thermally-induced image motion with a maximum excursion of one pixel in both the spatial and spectral directions during the course of a night. Larger shifts of a few pixels occur over the course of an observing run. As discussed in Section 7.2, the shifts during a night are easily corrected by tracing the positions of the fiber spectra and by tracking the positions of night sky emission lines. During August 2005, we will replace the coated black cloth currently enclosing the bench spectrographs to prevent light leaks with light-tight insulated panels. This replacement will remove a potential fire hazard from the light-tight but flammable cloth and improve the thermal insulation in the spectrograph room.

6.3. Gravitational and Rotator-Induced Flexure of Fiber Positioner

Our finite element models of Hectospec predicted that the Hectospec’s focal plane assembly (onto which the fibers are attached) would shift by $\sim 50 \mu\text{m}$ relative to the robot’s gripper assembly as the telescope pointing changes from zenith to an elevation angle of 30° . This flexure is relevant because we use the robots to establish the correct position of the guide stars in the guider probes. We took advantage of a cloudy night to measure this flexure by placing the fibers on the focal surface at the zenith in the usual fashion, tipping the telescope in elevation, and measuring the position of the backlit fibers. The average deflections that we measured moving from an elevation angle of 90° to an elevation angle of 30° are $40 \mu\text{m}$ in one robot and $42 \mu\text{m}$ in the other. We also noticed that rotating the instrument rotator produces repeatable deflections of up to $25 \mu\text{m}$ if the elevation angle is held constant. Rotator-induced deflections were anticipated, and set stringent requirements

on the accuracy of the rotator bearing.

6.4. Observing Overhead

The elapsed time between completing an exposure on one field and beginning another is 1040 s. Table 3 lists the items that contribute to the observing overhead. The observing overhead will drop slightly with increased automation of the wave front sensing procedure, but is unlikely to drop much below 900 s.

6.5. Hectospec Reliability

Hectospec has proven to be reliable at the telescope despite its complexity. We have lost ~ 4 nights of observing time in Hectospec’s first year of operation due to instrument malfunctions. The most serious incident occurred in July 2004. A backlash removal spring in the gripper mechanism failed, and the gripper misplaced a button. During the diagnosis and recovery process, a series of low level robot commands were issued and the robots were inadvertently parked with a fiber caught in the gripper jaws. This event resulted in the spectacular destruction of the captured optical fiber. The damaged fiber was replaced with a spare fiber from one of the five spare groups of fibers, and the antibacklash springs in both grippers were replaced with longer springs of the same spring constant. Our analysis revealed that the original spring was repeatedly overstressed in normal operation. We have also revised our procedures to require visual inspection of the Hectospec focal plane and fiber positions before executing low level robot commands.

Two of the other Hectospec malfunctions involved the guide probes. During the first incident, the guider probe braking mechanism on one of the probes stuck open, causing the guide probes to fall out of position as the telescope was slewed away from the zenith.

The problem was traced to excessive friction on the brake guide shafts which was removed by polishing the shafts on all three guider probes. The second incident was caused by the guider brake failing to release on one of the guider probes. This problem was traced to a loose connector, which was possibly not fully seated following the brake shaft rework.

7. Hectospec Data Analysis Pipeline

7.1. Introduction

The ~ 5000 spectra produced nightly by the Hectospec are reduced using a semi-automated pipeline; typically this reduction is completed by the afternoon following the observations. The reduction yields a catalog of redshifts, errors, signal to noise estimates and crude spectral types in time to modify the next nights observing plans, if necessary. Mink et al. (2005) give an overview of the entire data flow, from forming the observing catalog to archiving and releasing the final reduced spectra. Here we describe those steps taken to reduce the raw CCD frames into a set of wavelength calibrated spectra with redshifts. The system rests on the IRAF spectral reduction packages (Valdes 1992) and the IRAF task **dofibers** (Valdes 1995). The process is controlled by a set of custom IRAF CL scripts, similar to those which control the reduction of data from the FAST spectrograph (Tokarz & Roll 1997).

7.2. Wavelength Calibration

Accurate wavelength calibrations are crucial to the performance of fiber spectrographs on large aperture telescopes. Small wavelength calibration errors cause artifacts in the subtraction of the near infra-red OH night sky lines which mask or mimic the appearance of H α emission at $z \geq 0.2$. In a one hour exposure Hectospec is routinely able to measure

spectra for galaxies with central I band surface brightnesses 10% of the night sky brightness.

Our basic wavelength calibration procedure consists of fitting the centers of emission lines produced by our Fe-cathode NeAr hollow cathode lamp with a low order polynomial, once for each fiber, following the standard procedures in **dofibers**. Typical scatter about these fits is 0.06 \AA , consistent with the error in determining individual line centers. A single set of (typically) five calibration exposures is taken in the late afternoon, with eight NeAr lamps illuminating panels on the MMT’s building shutters.

The next step in the procedure corrects for thermally induced spectral shifts. Purely linear image shifts can be removed easily. Figure 17 shows the image motion in the dispersion direction for a typical week of observing in April 2005. These shifts are obtained by cross correlating a 1000 \AA wide image section centered near the $\lambda 8399 \text{ \AA}$ night sky line taken from the first on-sky CCD frame taken each night; thus the drift shown in figure 17 is reset to zero each night. Typical nightly image motion is less than one pixel. The image motions in the direction perpendicular to the dispersion show similar patterns and extents; the two components of motion are not strongly correlated.

Any non-linear shifts would appear to first order as stretches or rotations. Figure 18 shows the differences in the shift as measured by cross correlation of image segments centered around $\lambda 8399 \text{ \AA}$ and around $\lambda 5577 \text{ \AA}$ for the same week in April 2005 shown in Figure 17. Notice that the y axis scale has been expanded by a factor of five. The results are consistent with zero distortion within the measurement error of 0.02 pixels. A similar analysis shows that image rotations are also consistent with zero. A systematic change in the image scale of one part in 100,000 over twelve hours would result in a change in the measured distance of 0.02 pixels between $\lambda 8399$ and $\lambda 5577$. This is the level of the scatter in figure 18, and represents a lower limit on the image stability.

While the shifts measured by direct image correlation could put all on-sky images onto

the same system before the extraction of the 1-D spectra, this procedure would not solve the problem of putting the on-sky images onto the same system as the NeArFe calibration spectra. We choose to make the correction after the (curved) 1-D spectra have been extracted, but before they are rebinned into wavelength space. Compared with shifting before extracting this correction induces an error which is proportional to the sine of the difference in the angle of curvature of the spectra between the NeArFe spectrum and the on-sky spectrum, at each fixed pixel position. For image shifts of \sim one pixel, even for the most highly curved spectra, this error is negligible compared with the other sources of error.

We use the standard **apextract** techniques, determining the shift perpendicular to the dispersion direction by image correlation with the flat field image (which must be taken at nearly the same time as the NeArFe calibrations). After extracting the 300 spectra from the image we simply measure the centroid of the $\lambda 5577$ night sky line, in pixel space, and calculate (for each spectrum) the shift, in pixels between that position and its expected position, as determined from the (300) NeAr solutions. We assign the median shift to be the shift in the dispersion direction for the entire image, and modify the wavelength polynomials accordingly. Finally, we rebin the spectra into equal wavelength pixels.

Figure 19 shows the pixel shifts for each spectrum on the night of 10 April 2005, which is broadly typical. Each point represents one spectrum, and each set of 300 points represents one CCD frame. The spectra from each frame are plotted in order, the time between frames is not shown, but can be seen in figure 17 (the night in figure 19 is the second night from the right). Three things are apparent in figure 19. (1) The shifts in the position of $\lambda 5577$ are large when compared with other effects. (2) The shifts change smoothly, but with occasional discontinuities resulting from **apextract**'s choice of zeropoint. The discontinuities demonstrate clearly that the shifts must be corrected before spectra may be combined. (3) Finally, each set of 300 spectra, from a single frame, shows small, systematic

differences in the shift as a function of position in the frame. The amplitude of this shift, from top to bottom, is similar to the scatter in the measurement of a single line center. The origin of this shift is unknown, but it is not due to systematic errors in the wavelength polynomial. We currently do not correct for this small effect.

Figure 20 shows the final measured positions for the $\lambda 8399$ Å night sky line after the spectra from figure 19 have been wavelength calibrated and rebinned into 1-Å-wide equal wavelength bins. The scatter about the expected value is 0.092 Å, which includes the small systematic errors seen in Figure 19. The offset of 0.075 Å is approximately constant throughout the night, and may be attributed to errors in the calibration polynomial as there is no apparent drift.

7.3. Sky Subtraction

The removal of the night sky spectrum from observations of faint objects made with fiber optic spectrographs has long been viewed as problematic (e.g. Wyse & Gilmore (1992), Lissandrini et al. (1994), Watson et al. (1998)). Recently methods have been developed which fit local variations from the mean sky due to changes in fiber transmission, focus, etc. by means of eigenvector techniques Kurtz & Mink (2000), and B-splines Marinoni et al. (2001). The stability of Hectospec’s bench spectrograph allows us to reach near Poisson limited sky subtraction without having to resort to the use of eigenvectors or B-splines.

Typically 30 Hectospec fibers (10% of the total) are allocated to blank sky observations. We reduce the data for each of the two CCD chips separately because combining sky spectra from the two chips degrades performance. The point spread functions of the two CCDs differ by ~ 0.2 pixels FWHM, apparently due to differences in the CCD charge diffusion.

We check for objects contaminating the sky spectra in two ways. (1) We divide each

sky spectrum by the mean of all the sky spectra. When the RMS pixel value exceeds a threshold the sky spectrum is considered contaminated, and is rejected. (2) We subtract the (revised) mean sky spectrum from each remaining sky spectrum, then correlate the residuals against our absorption and emission line galaxy templates; spectra which yield significant redshifts (significance is determined by the Tonry & Davis (1979) r statistic) are contaminated by galaxian or stellar light, and are rejected. For a typical sample, taken in March and April 2005, 181 of 972 sky spectra ($\sim 19\%$) were found to be contaminated by this test.

We subtract the sky from each object spectrum by averaging the six closest (clean) sky spectra. We rescale this average so that the flux in the OH 8399Å line matches the flux in the object spectrum, and then simply subtract the rescaled sky spectrum from the object spectrum. For galaxies with $R \sim 20$ this procedure works very well. We test the limits of the technique by applying it to the measurement of substantially fainter spectra.

We chose 222 objects from a deep galaxy survey (Dell’Antonio et al. 2005) that were evenly distributed in $V - R$ color between $0.0 < V - R < 1.3$. One third were evenly divided in bright magnitude $21 < R < 22$ and two thirds were evenly divided in faint magnitude $22 < R < 22.5$; figure 21 shows the distribution of objects. These objects were observed in two different Hectospec configurations before and after transit. The first observation had 160 minutes exposure and the second 120 minutes exposure. The two data sets were reduced separately, then summed to provide the final spectra. We obtained reliable redshifts for 137 of these objects; the remainder had insufficient signal to noise to obtain redshifts. The solid dots in figure 21 show the galaxies with redshifts; they tend to be brighter and bluer.

Figure 22 shows the success rate as a function of the $1.5''$ diameter aperture magnitude, which corresponds to the light down the fiber. The success rate falls rapidly for objects fainter than $R_{1.5''} = 23.0$; essentially all of the lower central surface brightness objects with

reliable redshifts are emission line objects.

Figure 23 shows a 280 minute exposure spectrum of a galaxy at $z=0.71$ having with $R=22.0$ and $R_{1.5''}=22.97$ prior to sky subtraction. Figure 24 shows the spectrum after sky subtraction and after application of an 8 \AA smoothing window. The CaII K line for this galaxy is detected in absorption at $\sim 1.5 \sigma$ significance. There are about 450 independent 10 pixel wide regions in this spectrum, we would expect about 30 of these to have positive fluctuations greater than the size of the K line, and 30 to have negative fluctuations. This behavior is approximately what we see in this spectrum, taking into account that the intensity of the sky radiation (and thus the size of the statistical fluctuations) is in some places substantially higher than at the location of the K line.

The coincidence of several features allows a reliable redshift to be determined in this case, but the existence of many similar sized noise spikes suggests that the spectrum of this $R \sim 22$ galaxy is near the limit. Were this object at $z=1.0$ the light entering the fiber would be reduced by half and the spectral lines would be redshifted into the OH night sky line forest. With perfect sky subtraction the K line would be about a 0.3σ effect; redshift determinations are impossible at these levels. While in theory substantially longer exposures could be made to measure higher redshift objects, in practice it makes more sense to use higher resolution to isolate the night sky features (Davis et al. 2003). A 600 line grating blazed in the red for the Hectospec will see first light during the second half of 2005.

8. Typical Hectospec Performance in Survey Mode

Hectospec is frequently used to observe objects with $R < 21.0$ with exposures of 30 to 120 minutes. Often observations are made with partial moon. Figures 25 and 26 show representative 60 minute exposures, taken with the moon up, six days past the new moon.

Redshifts are determined using the methods described by Kurtz & Mink (1998), hereafter KM98. New templates, using objects with $z \sim 0.3$ were created for the correlation analysis, as described in KM98.

Figure 27 shows the relation between isophotal R magnitude and the Tonry & Davis (1979) r statistic, a measure of redshift quality, for 1455 absorption line galaxies observed with one hour exposures (some with moon) in March and April 2005 as part of the gravitational lensing survey (Geller et al. 2005). All these spectra yielded reliable redshifts. There is little correlation between the magnitude and the quality of the redshift.

Figure 28 shows the same 1455 absorption line galaxies, but with the $1.5''$ aperture magnitude, which represents the light down the fiber, vs. the r statistic. As expected there is now a strong correlation. The Mt. Hopkins R band dark sky brightness is typically 20.0 in a $1.5''$ aperture (Massey & Foltz 2000; Patat 2003). The Hectospec routinely obtains absorption line redshifts for objects at 20% of the sky in one hour exposures.

Following KM98 we use 332 objects with duplicate spectra to estimate the error in a redshift measurement as a function of the r statistic. We find that the median velocity error for absorption line redshifts can be described by $\Delta v_{abs} = 130/(1 + r) + 5 \text{ km s}^{-1}$ while the emission line redshift errors can be described by $\Delta v_{em} = 100/(1 + r) + 5 \text{ km s}^{-1}$. The mean errors are about twice these, and are well represented by the normal **xcsao** error estimator (KM98).

9. Discussion and Conclusions

Hectospec is a powerful, wide-field spectrograph that makes excellent use of the converted MMT’s 1° diameter and 6.5 meter aperture. It reaches to $R=21.5$ with ease, and the sky subtraction with standard data reduction allows quality spectroscopy to $R=22$ with

sufficient exposure. Fiber spectrographs have an unjustified reputation in some quarters for compromised throughput that is probably due to design shortcomings in the fiber run between the focal plane and the spectrograph and in the design of bench spectrographs. Hectospec’s peak system throughput of 10% including aperture losses, and 17% correcting for aperture losses, is quite competitive with slit spectrographs when its huge multiplex advantage is taken into account. A high-throughput long-slit spectrograph like the FAST spectrograph on the Whipple Observatory’s 1.5m Tillinghast Reflector (Fabricant et al. 1998a) has a peak system throughput (correcting for aperture losses by using a wide slit) that reaches 30% with fresh mirror and corrector coatings, but is more typically $\sim 25\%$ in average conditions.

Hectospec is a popular instrument at the MMT. Users respond favorably to the flexibility and efficiency of the queue observing mode. We designed Hectospec to rapidly survey normal intermediate redshift galaxies and high redshift active galaxies identified through by space X-ray and infrared observatories, and these are active areas of research with Hectospec. A wide variety of other programs are underway, including several stellar programs. Because Hectospec can offer effective sky subtraction to $R \sim 22$, essentially limited by Poisson noise, it is a surprisingly versatile general-purpose spectrograph.

We are in the process of building a complementary optical imaging spectrograph for the MMT (Binospec, Fabricant et al. (2003)). A wide-field imaging spectrograph will allow us to efficiently survey galaxy dynamics at intermediate redshifts and will offer very high throughput (potentially twice Hectospec’s) and even more precise sky subtraction for very faint objects. However, Binospec’s advantages come at a price: its field of view is only 8% of Hectospec’s, and with likely slitlet lengths of $10''$ to $12''$, Binospec will offer $\sim 50\%$ of Hectospec’s multiplex advantage. The Hectospec will remain the instrument of choice for large surveys to depths of $R \sim 22$.

We are grateful for the contributions of the entire MMT instrument team, students, and of the MMT and Whipple Observatory staff. We thank Steve Amato, David Becker, Kevin Bennett, David Bosworth, David Boyd, Daniel Blanco, William Brymer, David Caldwell, Richard Cho, Shawn Callahan, Florine Collette, Dylan Curley, Emilio Falco, Craig Foltz, Art Gentile, Everett Johnston, Sheila Kannappan, Frank Licata, Steve Nichols, Dale Noll, Ricardo Ortiz, Tim Pickering, Frank Rivera, Phil Ritz, Rachel Roll, Cory Sassaman, Gary Schmidt, Dennis Smith, Ken Van Horn, David Weaver, Grant Williams and J.T. Williams. We thank the Hectospec robot operators: Perry Berlind and Mike Calkins, and the MMT operators: Mike Alegria, Alejandra Milone, and John McAfee. We are grateful to the efforts of the Harvard College Observatory Model Shop led by Larry Knowles. We thank Robert Dew and Diane Nutter of Cleveland Crystals and Terry Facey, formerly of Goodrich Optical Systems.

Facilities: MMT.

REFERENCES

- Barden et al. 1993, ASP Conf. Ser. 37: Fiber Optics in Astronomy II, 152, 185
- Blanco et al. 2004, Proc. SPIE, 5489, 300
- Callahan, S., Cuerdan, B., Fabricant, D., & Martin, H. 2004, Proc. SPIE, 5495, 228
- Davis, M., et al. 2003, Proc. SPIE, 4834, 161
- Dell’Antonio, I. 2005, private communication
- Epps, H. & Vogt, S., Appl. Opt., 32, 6272
- Fabricant, D. et al. 1998, PASP, 110, 79
- Fabricant, D. et al. 1998, Proc. SPIE, 3355, 285
- Fabricant, D. et al. 2003, Proc. SPIE, 4841, 134
- Fabricant, D. et al. 2004, Proc. SPIE, 5492, 767
- Fabricant, D., Hertz, E., & Szentgyorgyi, A. 1994, Proc. SPIE, 2198, 251
- Fata, R., Kradinov, V., & Fabricant, D. et al. 2004, Proc. SPIE, 5492, 553
- Fata, R & Fabricant, D. 1998, Proc. SPIE, 3355, 275
- Fata, R & Fabricant, D. 1994, Proc. SPIE, 2199, 580
- Fata, R & Fabricant, D. 1993, Proc. SPIE, 1998, 32
- Geary, J. 2000, *in Further Developments in Scientific Optical Imaging*, ed. Denton, M. B.,
(Cambridge, U.K.: Roy. Soc. Chem.)
- Geller, M. J. 2005, to be submitted to ApJ

- Kurtz, M. J., & Mink, D. J. 1998, PASP, 110, 934
- Kurtz, M. J., & Mink, D. J. 2000, ApJ, 533, L183
- Lissandrini, C., Cristiani, S., & La Franca, F. 1994, PASP, 106, 1157
- Marinoni, C., Davis, M., Coil, A. L., & Finkbeiner, D. 2001, in Where’s the Matter?,
Proceeding of the 3rd Marseille Cosmology Conference, eds. L. Tresse and M. Treyer,
p. 118, also astro-ph/0109164
- Massey, P., & Foltz, C. B. 2000, PASP, 112, 566
- Mink, D. M., Wyatt, W. F., Roll, J. B., Tokarz, S. B., Conroy, M. A., Caldwell, N., Kurtz,
M. J., and Geller, M. J., Astronomical Data Analysis Software and Systems XIV,
ASP Conference Series, in press.
- Parry, I & Gray, P. 1986, Proc. SPIE, 627, 118
- Patat, F. 2003, A&A, 400, 1183
- Pickering, T., West, S., & Fabricant, D. 2004, Proc. SPIE, 5489, 1041
- Roll, J.B. Jr., Fabricant, D., & McLeod, B. 1998, Proc. SPIE, 3355, 324
- Roll, J. 1996, ASP Conf. Ser. 101: Astronomical Data Analysis Software and Systems V,
101, 536
- Szentgyorgyi, A. et al. 1998, Proc. SPIE, 3355, 242
- Tokarz, S. P., & Roll, J. 1997, ASP Conf. Ser. 125: Astronomical Data Analysis Software
and Systems VI, 125, 140
- Tonry, J., & Davis, M. 1979, AJ, 84, 1511

- Valdes, F. 1995, “Guide to the Multifiber Reduction Task DOFIBERS,” IRAF On-line document; <http://iraf.noao.edu>.
- Valdes, F. 1992, ASP Conf. Ser. 25: Astronomical Data Analysis Software and Systems I, 25, 417
- Valdes, F. 1995, “Guide to the Multifiber Reduction Task DOFIBERS,” IRAF On-line document; <http://iraf.noao.edu>.
- Vogt, S. et al. 1994, Proc. SPIE, 2198, 362
- Watson, F., Offer, A. R., Lewis, I. J., Bailey, J. A., & Glazebrook, K. 1998, ASP Conf. Ser. 152: Fiber Optics in Astronomy III, 152, 50
- Wyse, R. F. G., & Gilmore, G. 1992, MNRAS, 257, 1

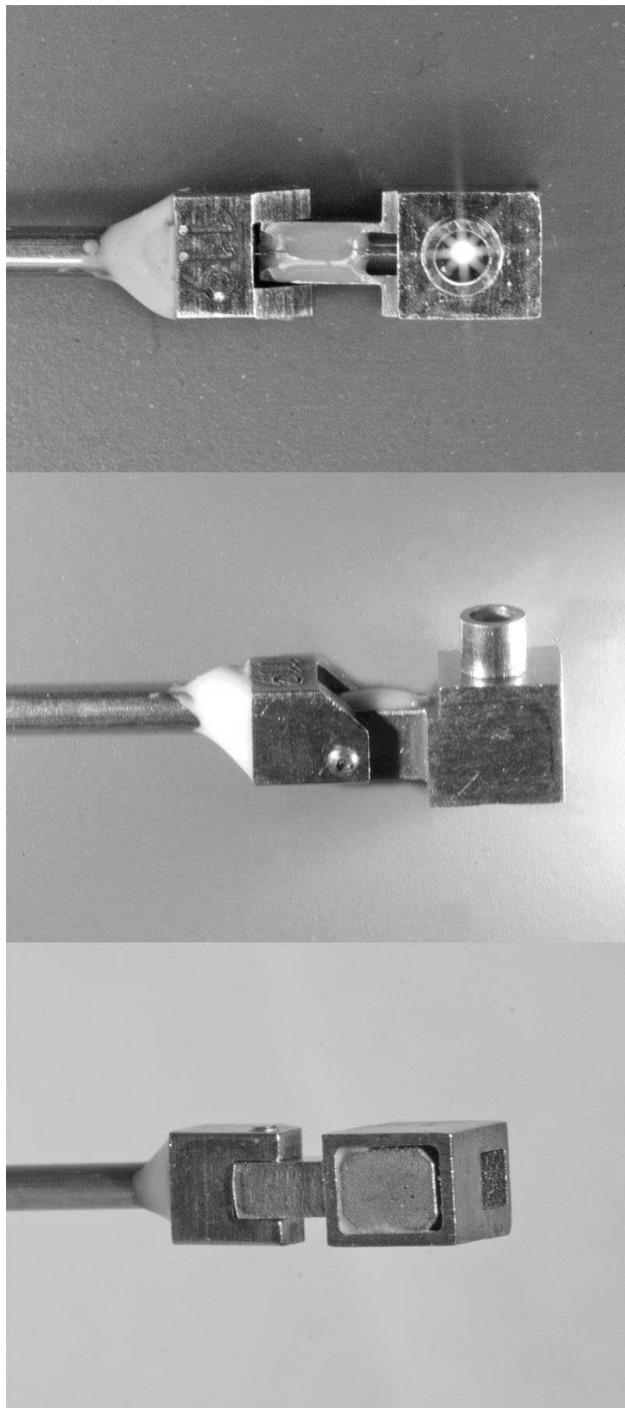


Fig. 1.— Three views of the fiber button assembly. Light from the backlit fiber is visible in the upper panel. The pivot point that allows the button assembly to accommodate the curved focal surface is visible in the middle panel. The rectangular NeFeB magnet bonded into the button assembly is visible in the lower panel.

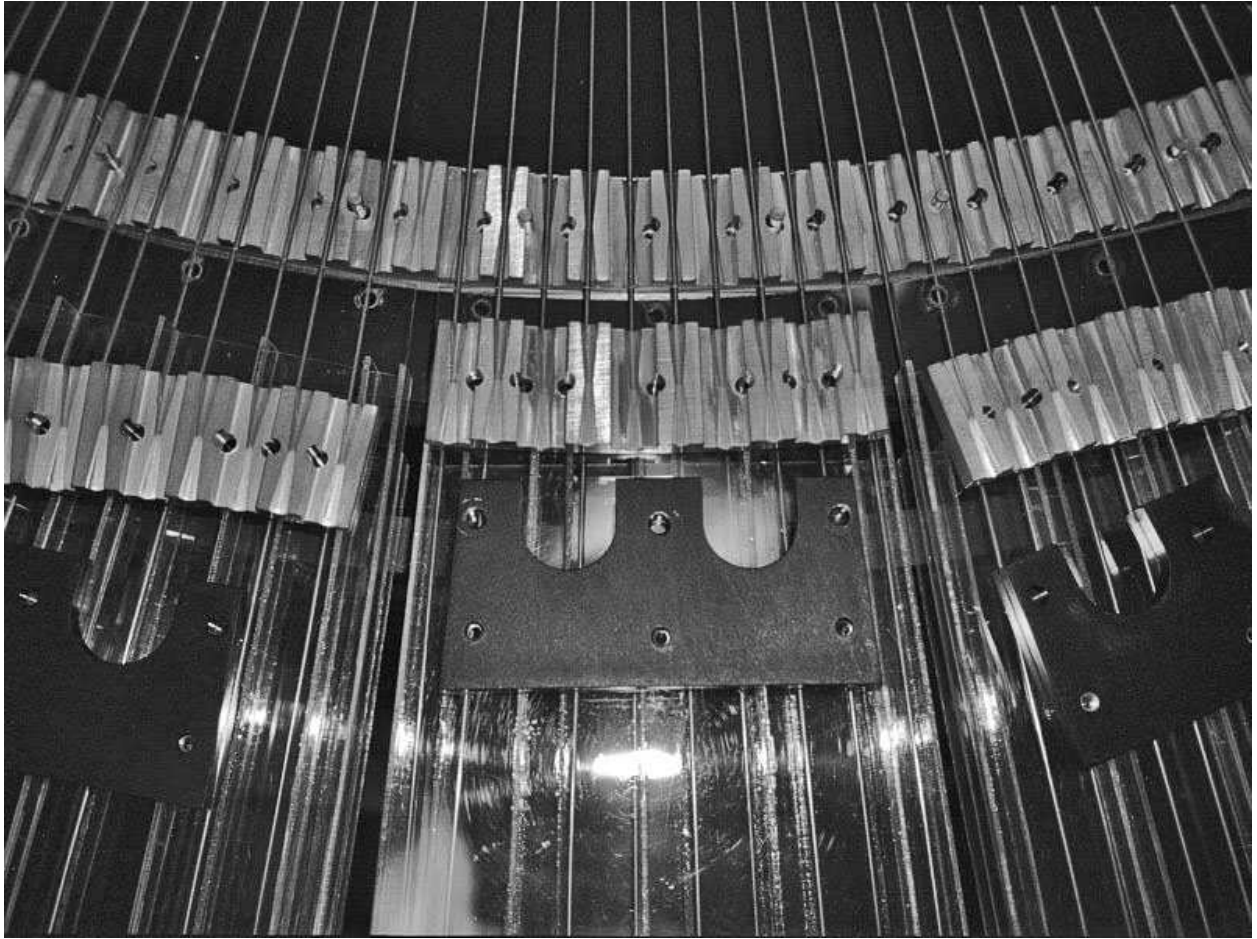


Fig. 2.— Disassembled fiber pivots. Pins register and screws hold the upper and lower halves of the fiber pivots together when the pivots are assembled. The pivot points are defined by the intersection of two cones. The pivots are arranged in two vertical levels so that the fiber syringes are fed into two vertical levels of separator trays.

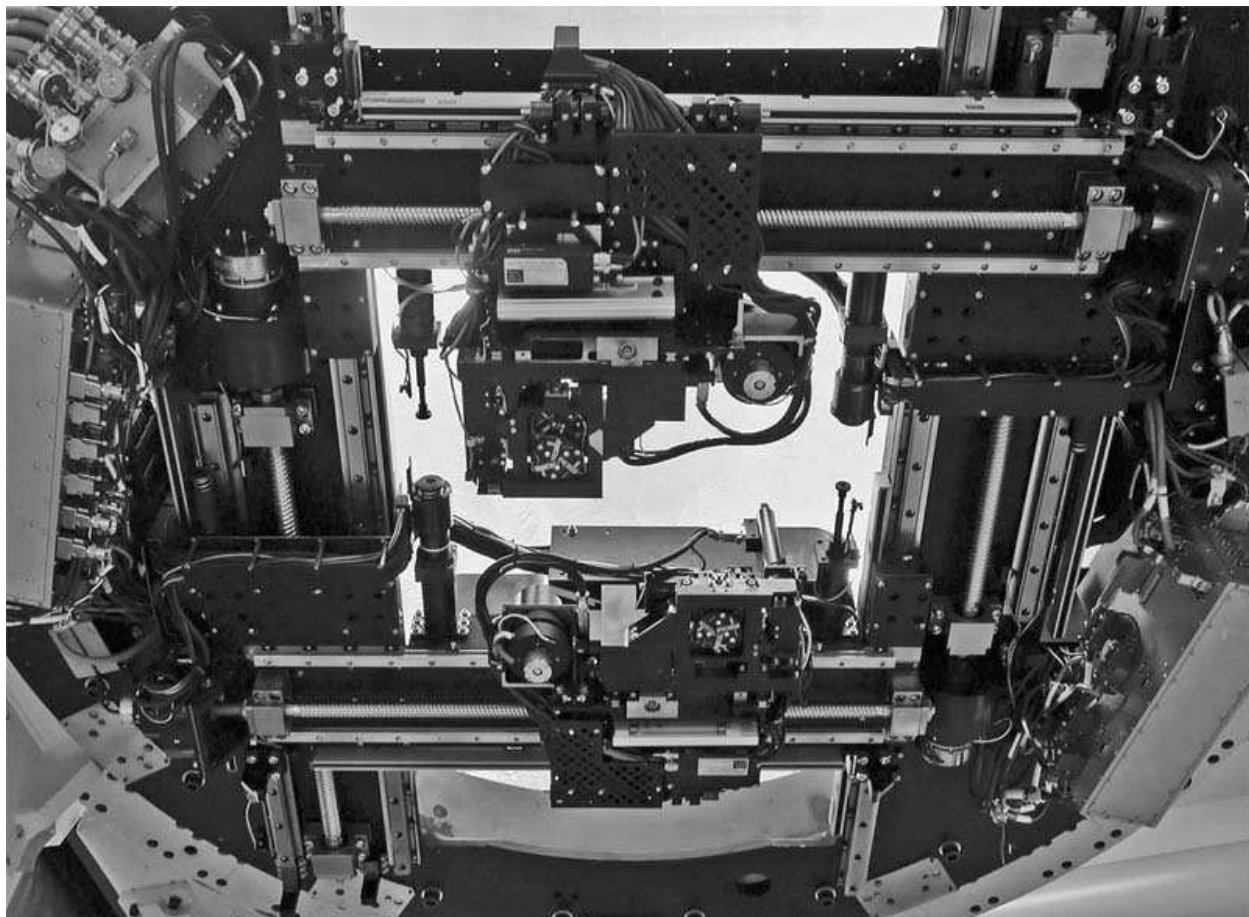


Fig. 3.— Upper unit of the fiber positioner. The X-axis stages and ball screws run vertically and the Y-axis stages and ballscrews run horizontally in this picture. The Z-axes run into the paper. The Θ gimbal axis tilts along the X direction, while the Φ axis tilts along the Y direction. The two grippers are the two circular assemblies near the center of the picture. The pair of X-axis collision bumpers are visible above and to the side of the two Z-axis assemblies.



Fig. 4.— Lower unit of the fiber positioner. This section of the fiber positioner can be unbolted from the upper unit that contains the robots (as shown). The lower unit contains the 300 fiber optic probes, the curved focal plate that holds the fiber optic probes, guide trays for the fiber probes, as well as the three guider probes (not visible).

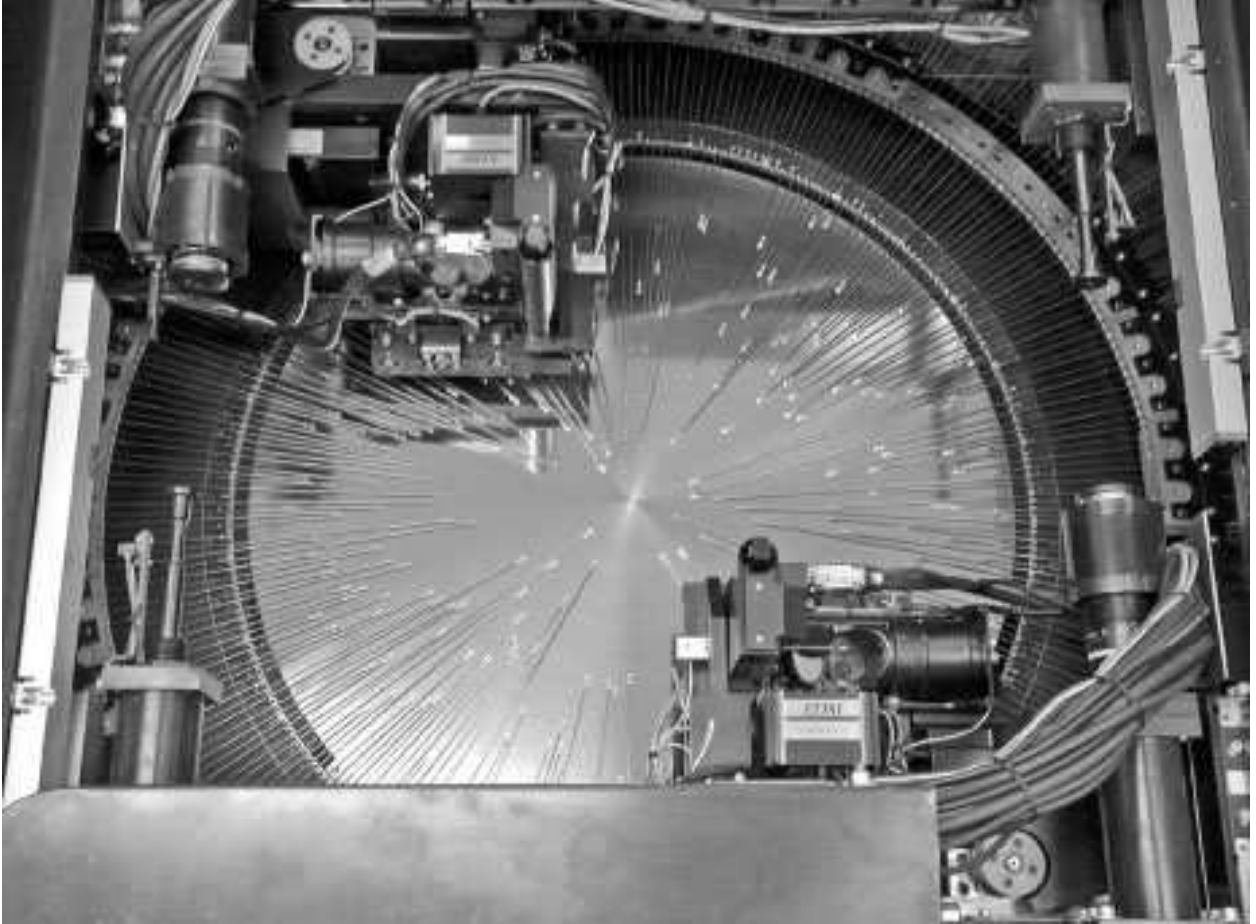


Fig. 5.— Top view of the assembled fiber positioner. This photograph was taken with upper cover assembly removed to allow a clearer view of the two six-axis robots. The X-axis collision bumpers are visible at the left and right. The two rectangular assemblies marked “EOSI” are the intensified TV cameras that travel with the robots. These TV cameras are used for calibration, alignment tests, and the initial acquisition of guide stars.



Fig. 6.— Z axis assembly of the fiber positioner. The Z axis motor, encoder and brake are visible at the center left. The cover for the metal drive band is mounted to the top of the Z axis motor assembly. The gripper jaws are visible at the lower right. The Θ axis actuator is located at the center right. The bearing assemblies for the Θ and Φ axes are located just above the gripper jaws at the lower right. The corner cube and fold mirrors for the robot TV cameras are located above the bearing assemblies.

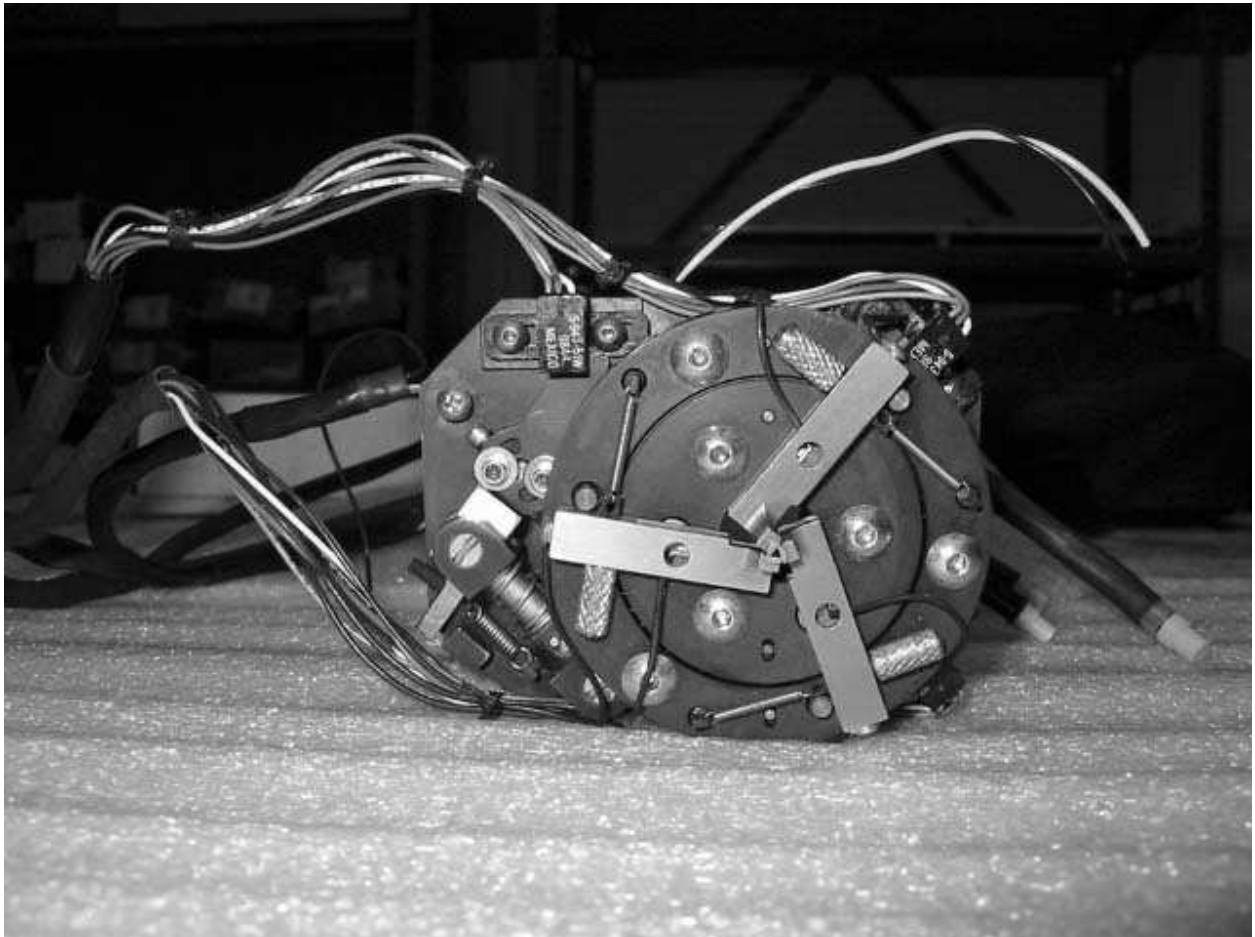


Fig. 7.— Gripper assembly used to pick and place fiber buttons. The three gripper jaws are actuated by a rotation of the outer ring to which the gripper fingers are attached, much like an iris mechanism.

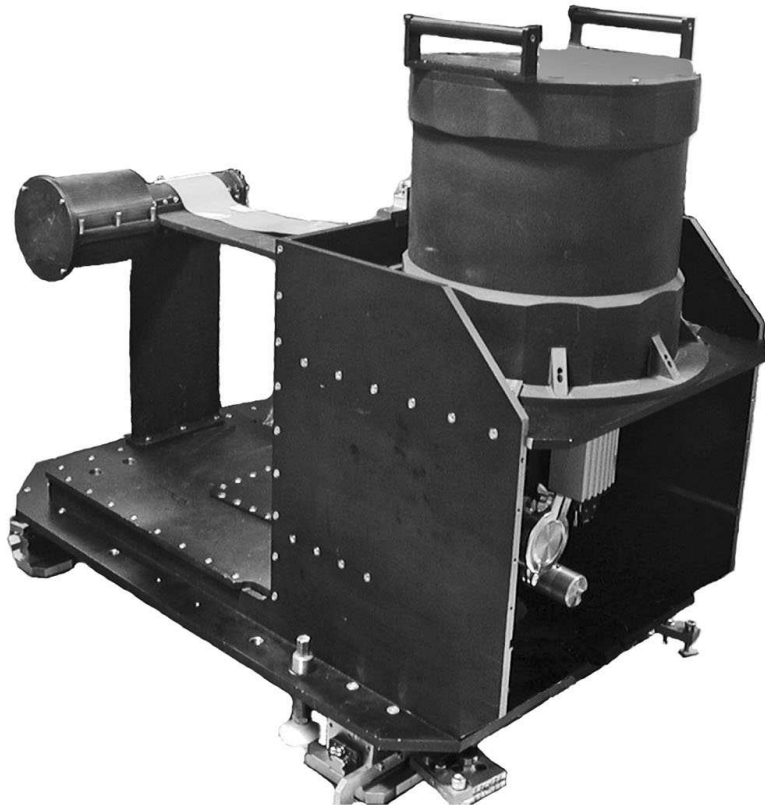


Fig. 8.— The Hectospec dewar assembly. The field flattener lens is obscured by a protective cover to the center left. The evacuated tube surrounding the cold finger runs horizontally. The LN₂ tank is prominent at the upper right.

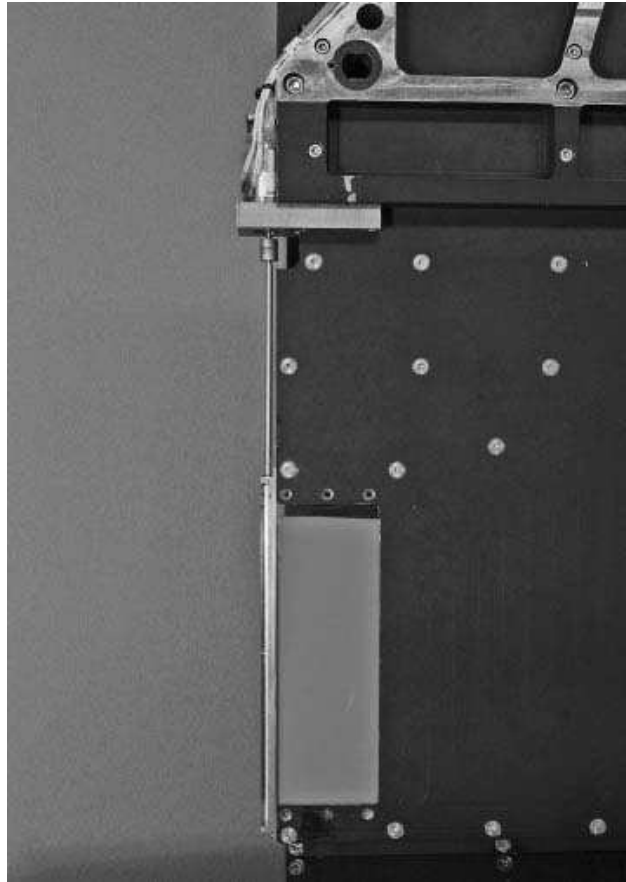


Fig. 9.— The rotary shutter assembly mounted on the fiber shoe. The small stepper motor used to drive the shutter is visible at the top center. This motor is coupled to the rotary shutter mechanism with a long shaft. The shutter itself is located at the lower left.

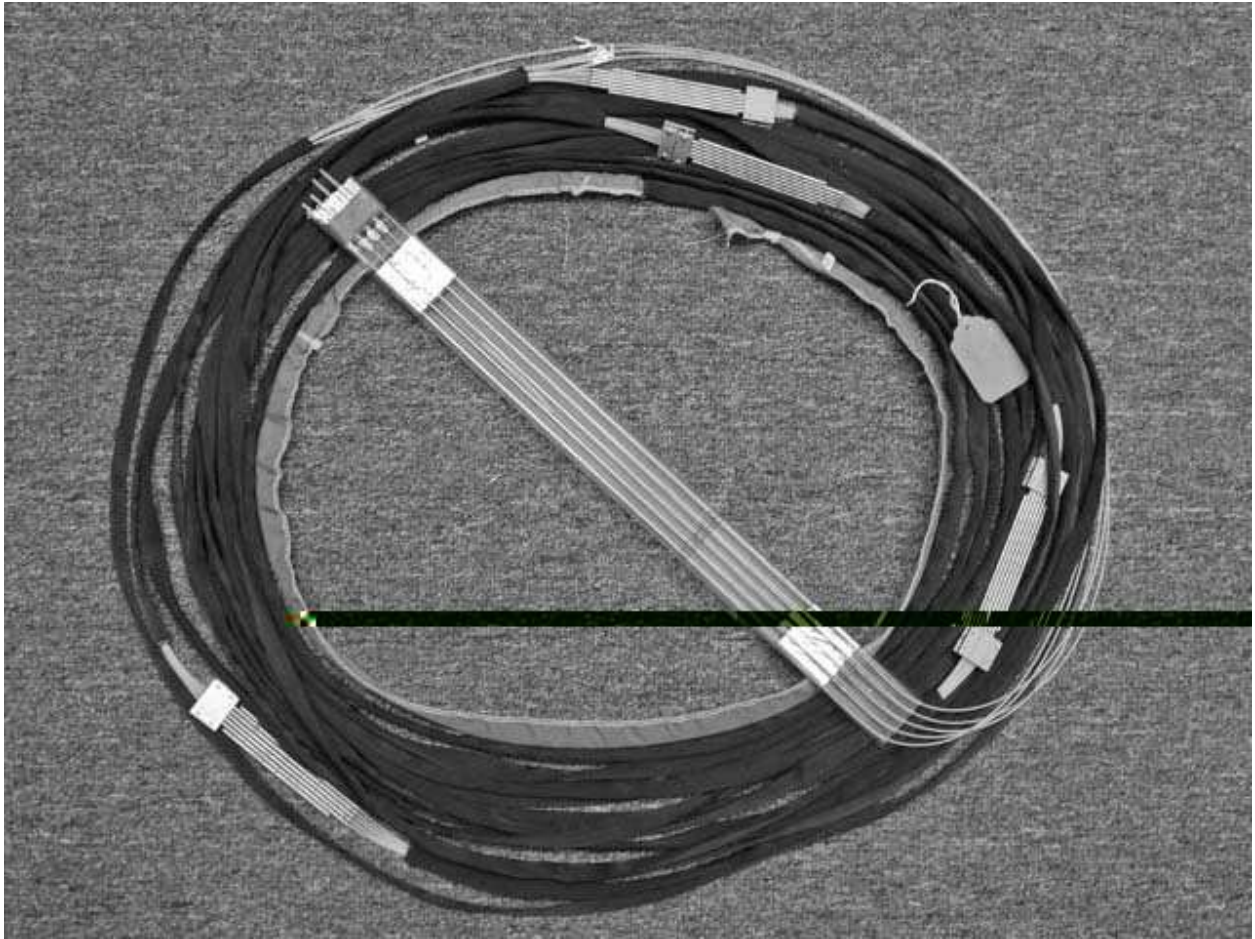


Fig. 10.— Coiled 26 m fiber run. The four thermal break assemblies are located at one, four, and eight o'clock. The fiber probe assemblies, protected by plastic tubes, are laid across the center running from the lower left to the upper right.

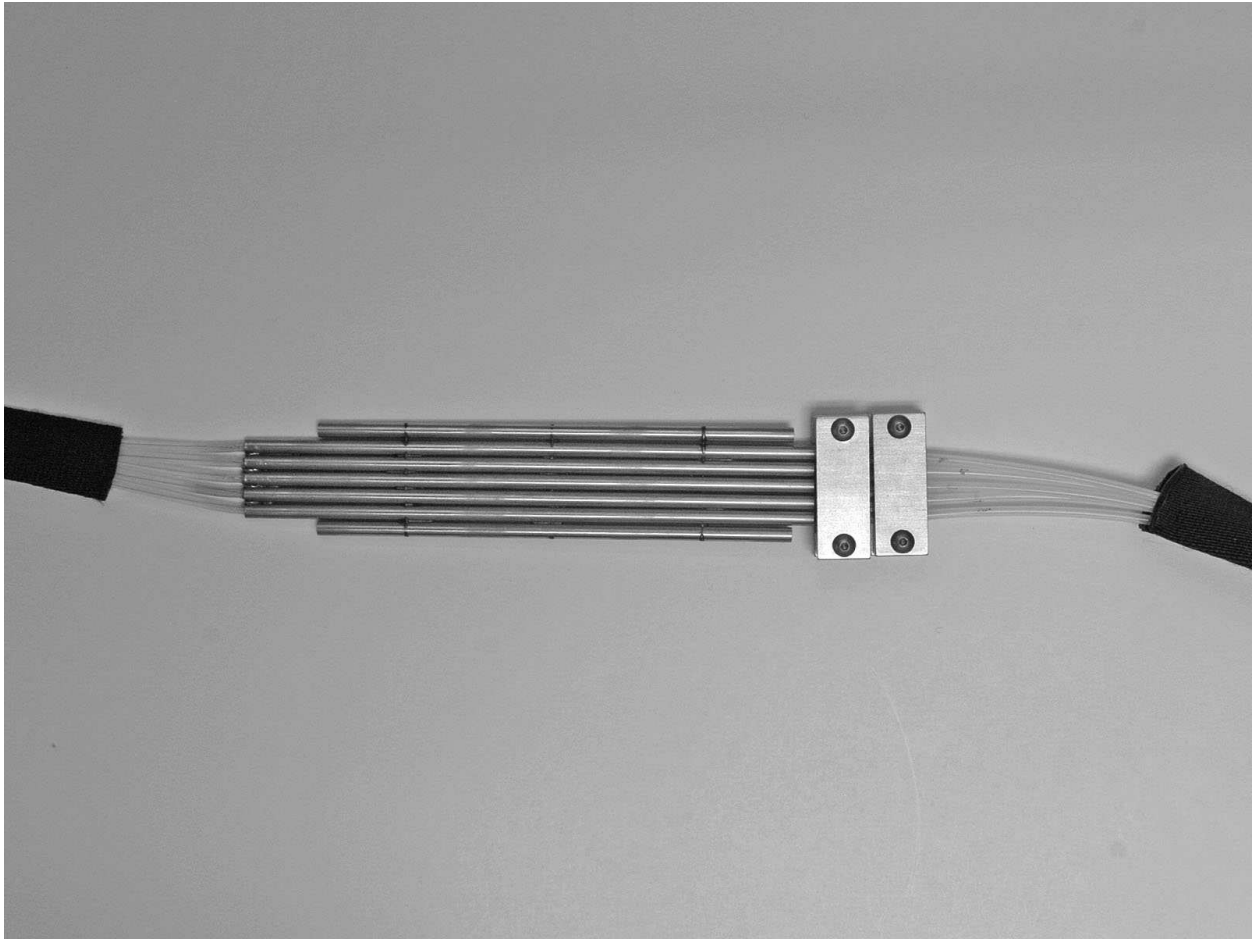


Fig. 11.— One of four fiber thermal breaks in the fiber run. A shipping clamp restraining the separation of the teflon tubes from the stainless thermal break tubes is in place at the right.

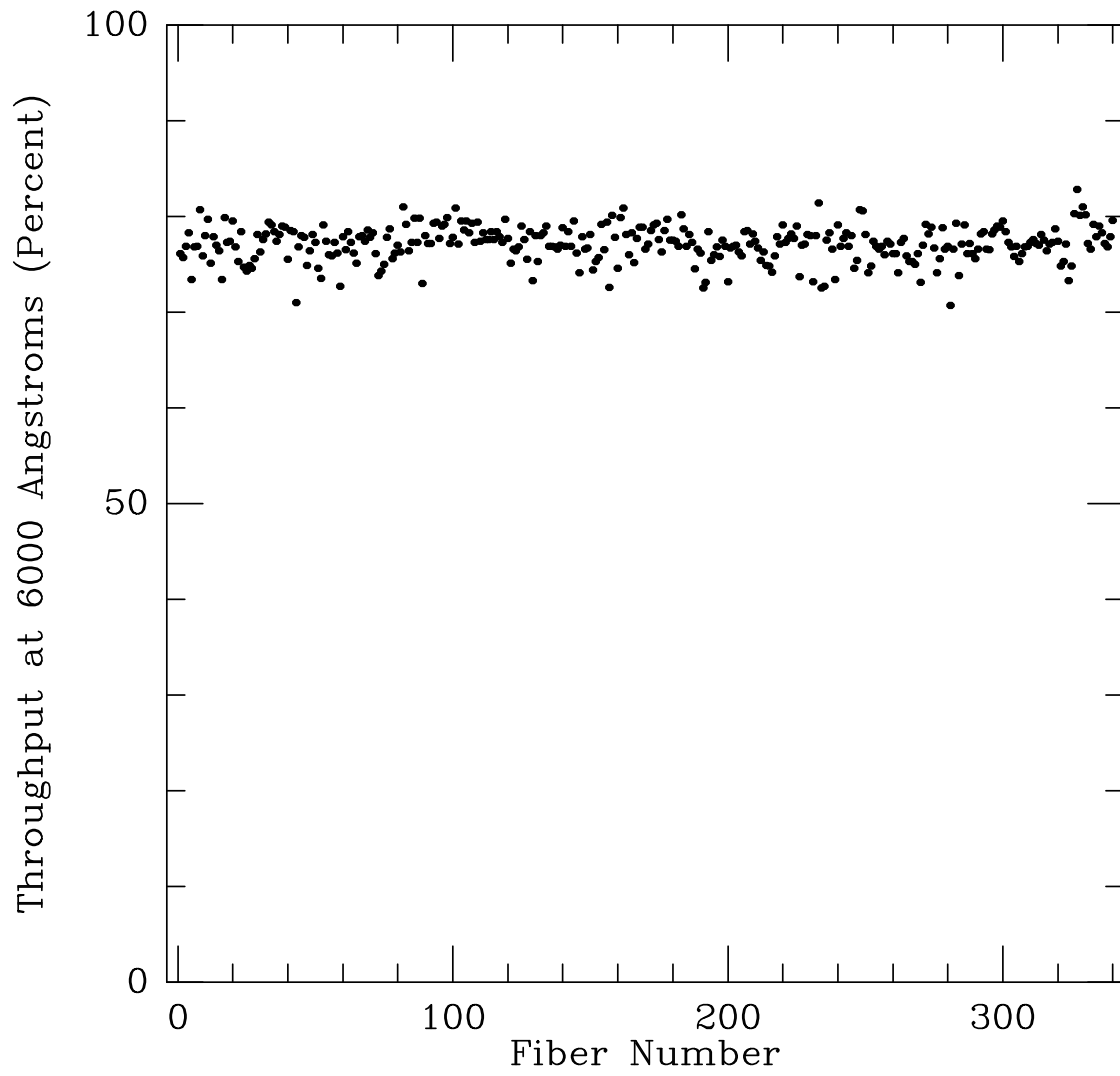


Fig. 12.— Fiber throughput at 6000 Å as measured in the laboratory.

Camera 1 is	Off	Gain	0	70	Set	Cal Off	Fid Off	R1 Offline	R2 Offline
Camera 2 is	Off	Gain	0	70	Set	Cal Off		Hctserv Up	Reset PMACs
Camera 3 is	Off	Gain	0	70	Set	Hse Off		Snappy Up	Epbox Up
								Guidserv Up	ADC WFC

On Deck	Setup On Field	Standard Ops	ADC/WFC
---------	----------------	--------------	---------

Config	File	m15.allfinal		Number	1	Browse	
adjust fibs	start	10:15		time	1 hour	skymin	50
	UseUTC	May 24 10:44 2005				skymax	60
	BestPA	pa0	-48.838	rot0	-12.969	PrintGuides	r1star
	OnDeck	pa	-41.600	rot1	-8.402	PrintGuides	r1star
				rot2	-1.899	skys	50
Go to zenith	ra	21:30:07.6149		dec	12:10:01.110		pa1
before moving robots	lst	10:18:00		ha	-11:12:07.614		airmas
configure fibs	ut	01:30:36					
move guide probes	a1	326.02	a2	208.14	a3	80	SetAngles
Slew to field				SetBias			ClrBias
robots to guide	rlx	-273.649	rlly	-146.372	r2x	257.639	r2y
gain up on all	rlxc	-273.644	rllyc	-146.366	r2xc	257.643	r2yc
guide transfer	rlbox	4	r2box	3	GuideOnRobots	TransferBoxes	
stow robots							
gain down on all							
Start Over							

Fig. 13.— The main screen of the Hobserve GUI. **Hobserve** is a tcl/tk script that provides a step by step procedural interface that guides the robot operator through the procedure of calculating the appropriate fiber configuration for the chosen observing time, calculating the sequence of fiber moves required to attain that configuration, issuing the move commands to the robots, and setting up the guiding on the field with the preselected guide stars.

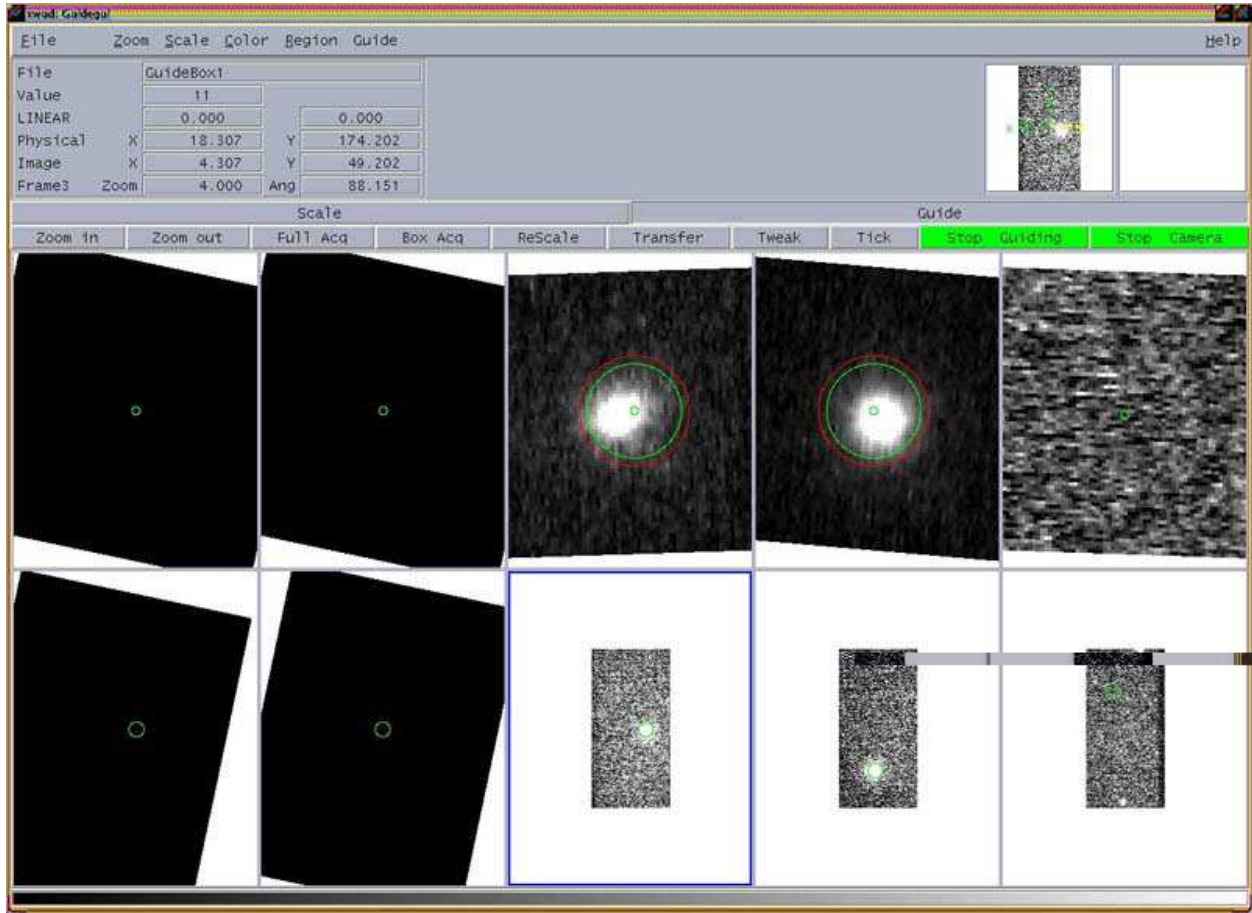


Fig. 14.— The guidegui display showing the guide star images from the guider probes and the reference positions. The robots are stowed during normal observations, so no guide stars are visible in the leftmost windows.

Pulizis	Estepow Up	Vacpow Up	Benchpow Up	Esaprepow Up				
Electronic Power	lvps1 on	lvps2 on	estoppow off	bkldgt off				
Bench Power	steppers on	hshutter on			Step Servers	Instserv Up	Homed	
CCD Power	camera on				CCD Servers	Detector Up	Hk Up	Heater Up
DomeBox Power	sw off	sw off	sw off	sw off	Dome Servers	Domecal Up		
					Telescope	Telescope Up	Wlcserv Up	Adc Up
					CCD temp	24.12	-21.80	VacGauge
					WaveFront	WaveFront Init	ADC	Vac on
					Dome Lamps	Continuous off	HeNeAr off	PenRay off
					Image Type	dummy	Exposure	ESTOP on
					Status	dummy	80 Shot	Track off
Status	Standard Ops	Auto Cal Ops	Sequence Tool	DomeCal Tool	Obislog Tool			
		Shutter	Grating	Focus	ZeroOrder			
Clear -->	shut idle		grat idle		focus idle			
CURRENT:	unknown		-0.009000		-0.001587			
TARGET:			-1.92%		0.015			
CALIBRATION:			-1.92%		0.015	3.402		
ConfigBench	FIELD:		parked					
TELNAME:	mmi f5 adc	INSTNAME:	hectospec	DETNAME:	specs			
OBSVRS:	DS, MC	P.I.:	calibration	PROPID:	calibration			
object1	Go	count	exptime	intcal				
		1	900	0				
Title	CLEAR *							
PAUSE Exposure	ABORT	RESUME	ABORT	RESUME				
PAUSE Queue	ABORT	RESUME	ABORT	RESUME				

Fig. 15.— The **SPICE** program provides a GUI interface to the spectrograph and camera controls and sequences the operations for various types of exposures. The GUI consists of two fixed displays at the top of the window along with several tab selectable displays that appear at the bottom of the window.

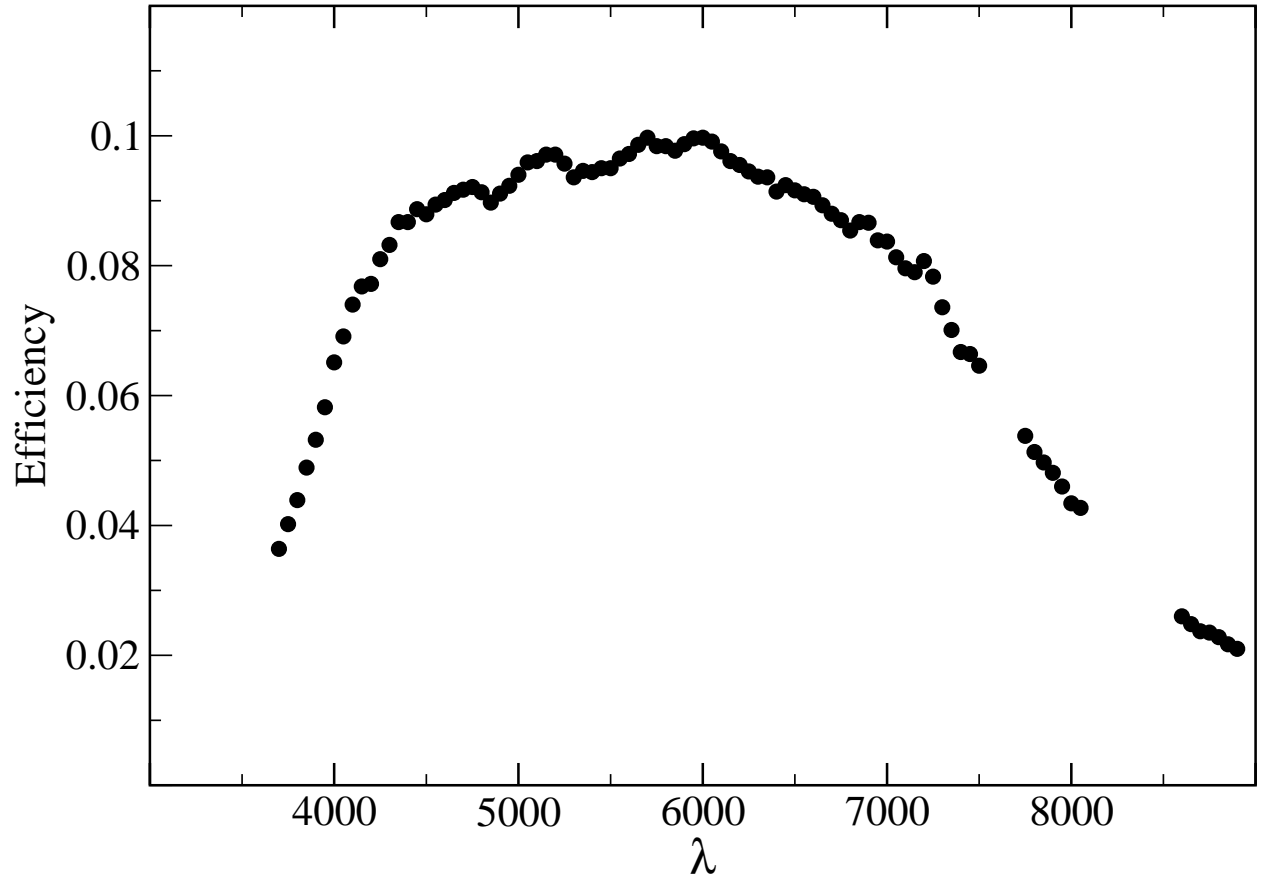


Fig. 16.— The measured system throughput as a function of wavelength in 1'' seeing. Aperture losses and losses in the telescope optics are included.

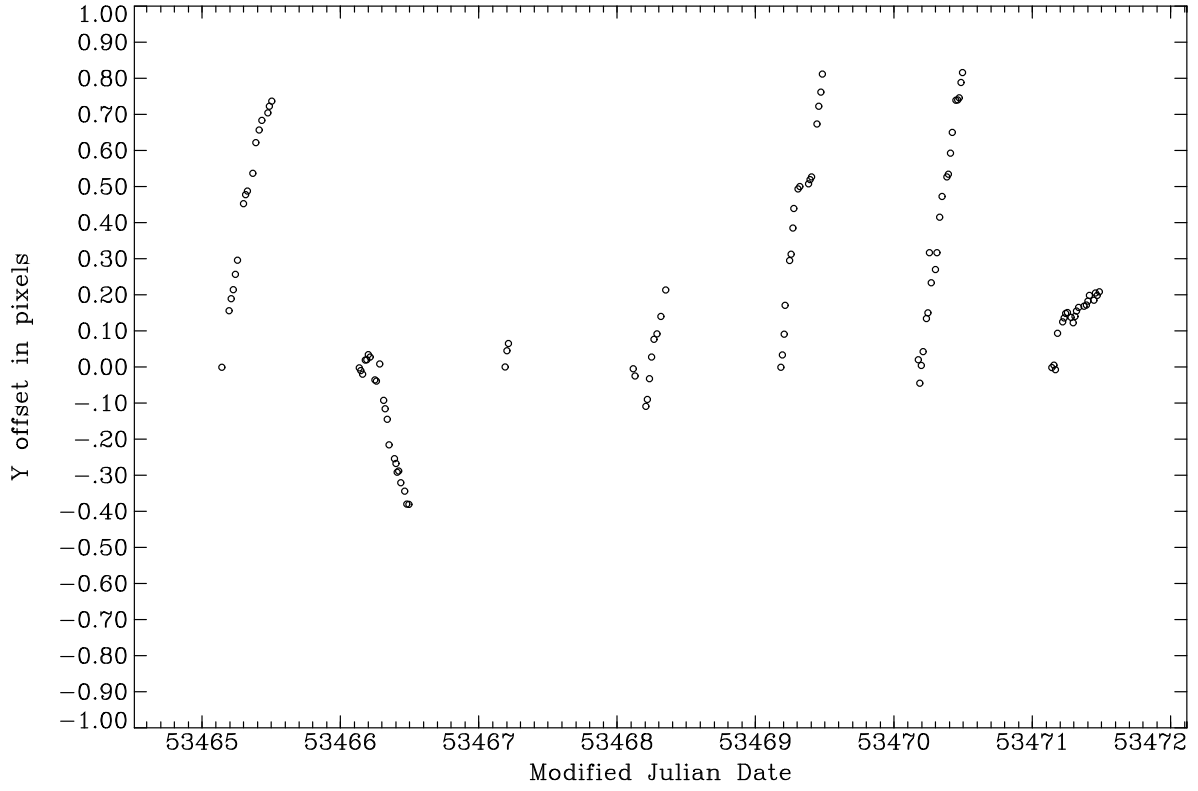


Fig. 17.— The image motion (shift) in the dispersion direction for the week following 5 April 2005. The shifts are calculated by image correlation and set to zero at the beginning of each night, as described in the text.

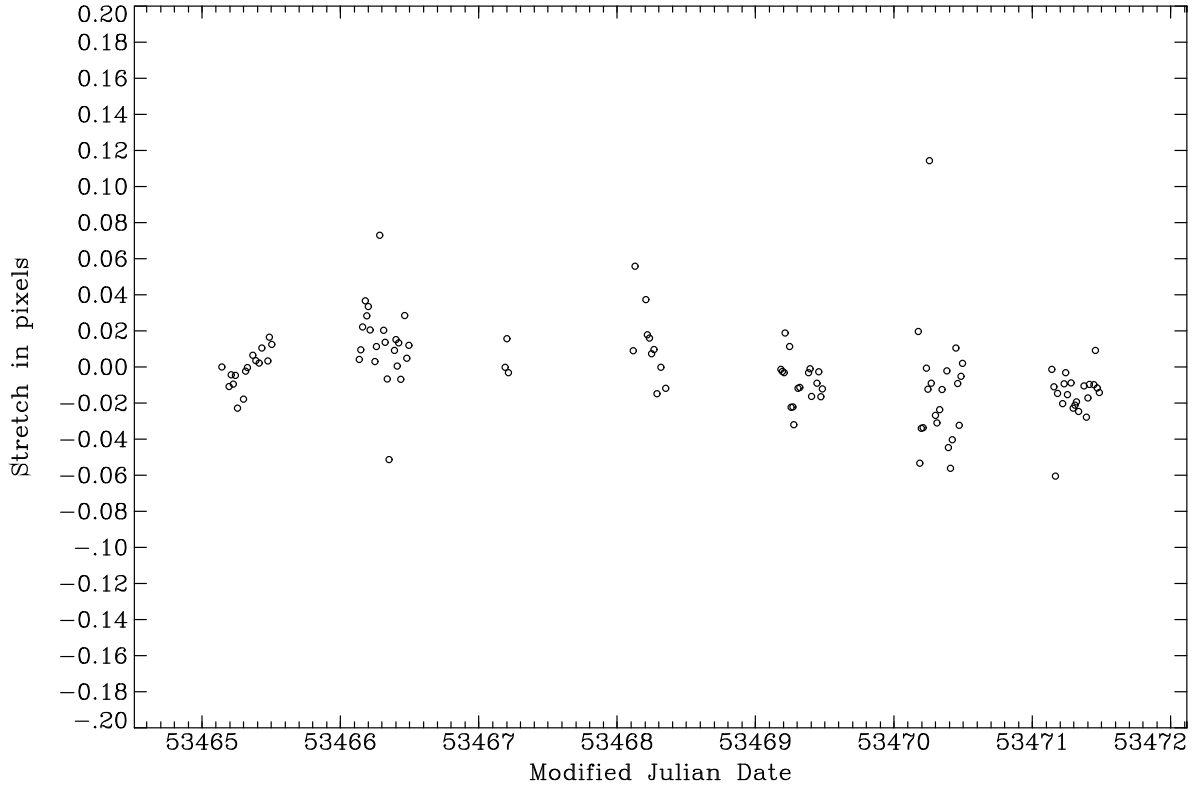


Fig. 18.— The stretch distortion in the dispersion direction for the week following 5 April 2005. The stretch is calculated by the difference in the red and blue image correlation shifts, and is set to zero at the beginning of each night, as described in the text.

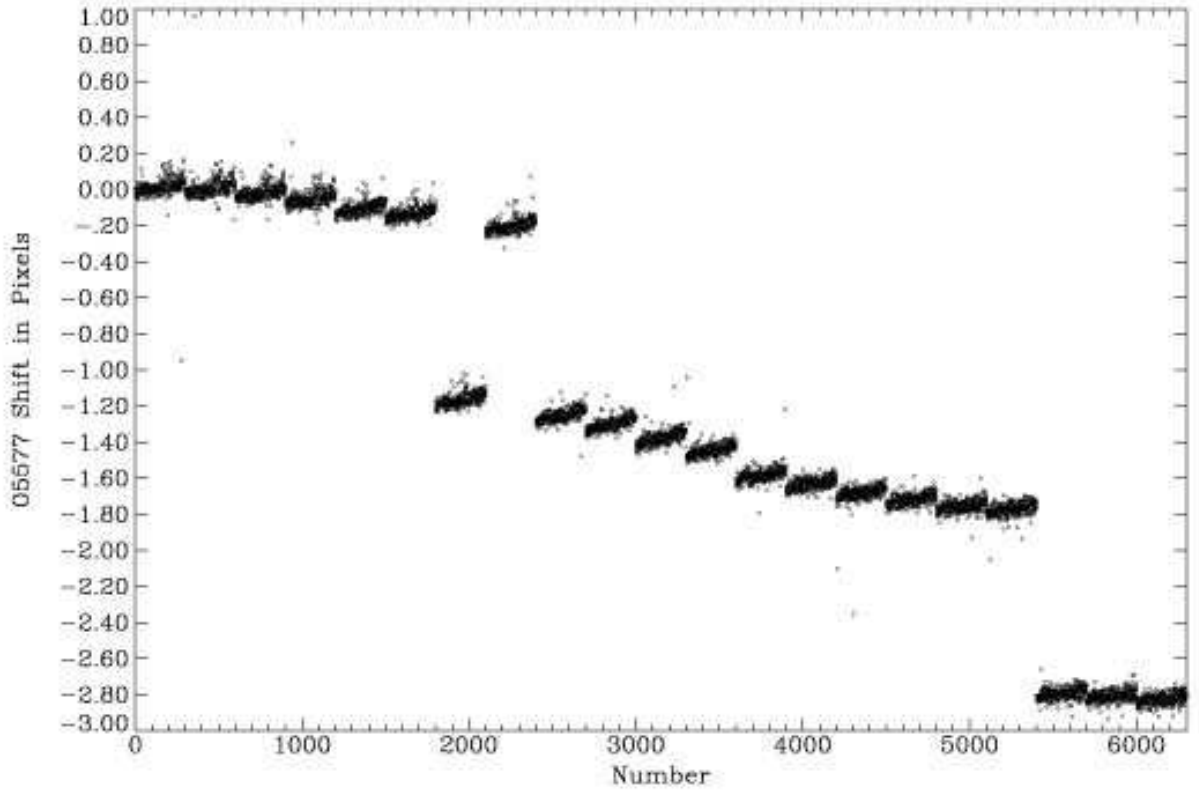


Fig. 19.— The measured position of the O[II] 5577 night sky line for each spectrum measured on 10 April 2005, after extraction into 1-D pixel space, but before the shift correction has been applied. The outliers in the plot are bad measurements due to cosmic ray hits near the sky line. No image combination to reject cosmic rays was performed to maintain high time resolution.

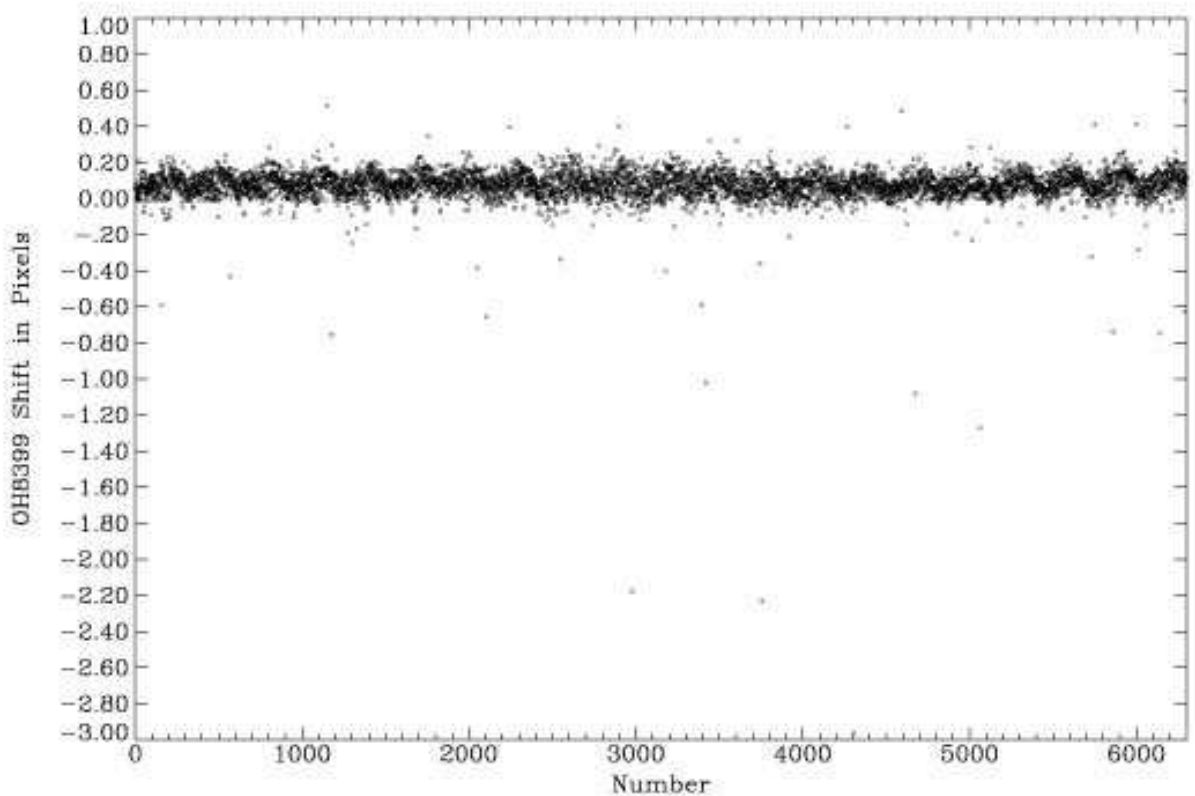


Fig. 20.— The measured position of the OH 8399 night sky line for each spectrum measured on 10 April 2005, after all calibration steps have been taken. The outliers in the plot are bad measurements due to cosmic ray hits near the sky line. No image combination to reject cosmic rays was performed to maintain high time resolution.

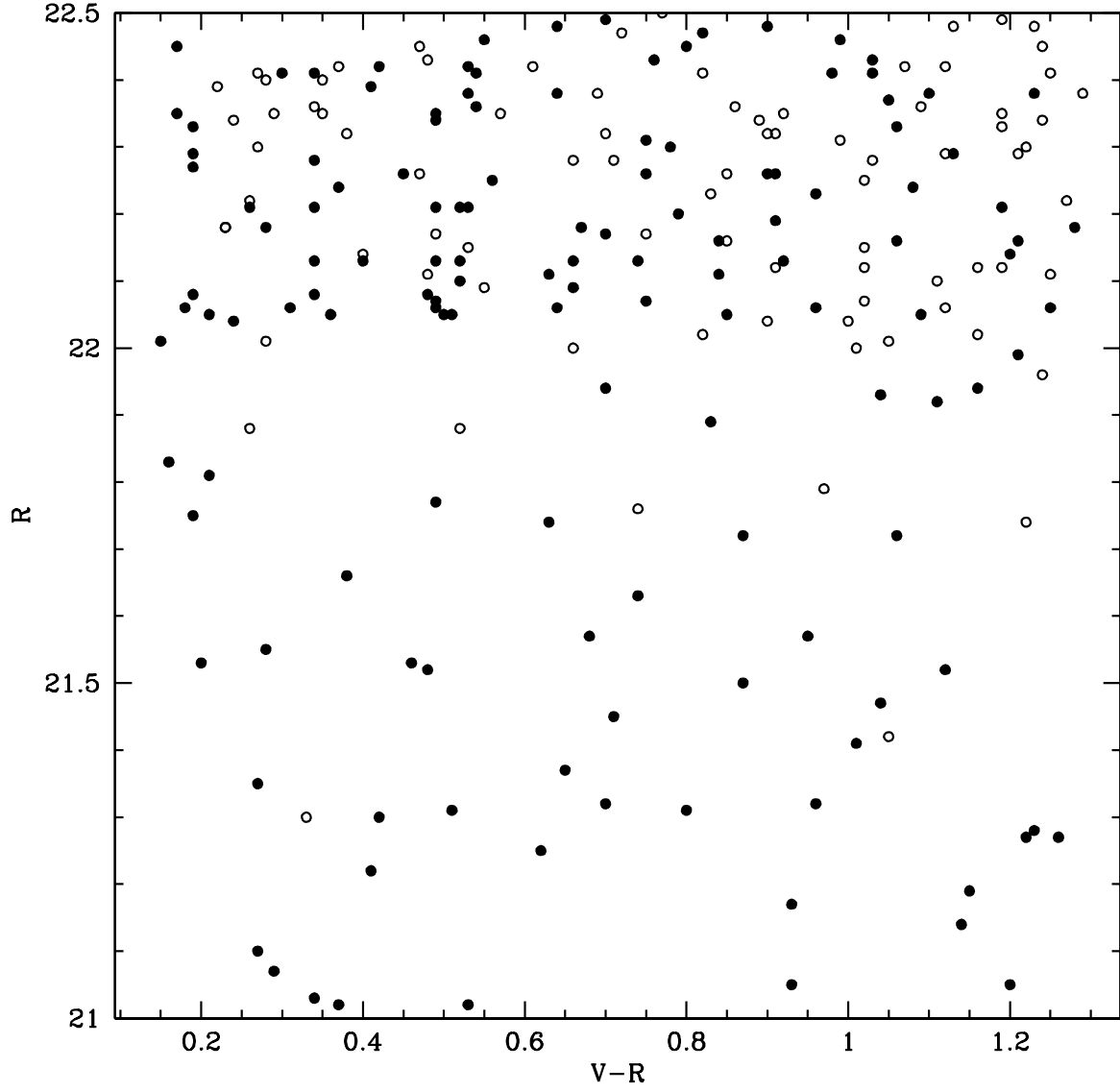


Fig. 21.— The distribution in $V - R$ color and isophotal R magnitude of the objects used to test the sky subtraction techniques; filled circles represent objects with reliable redshifts after 280 minutes exposure.

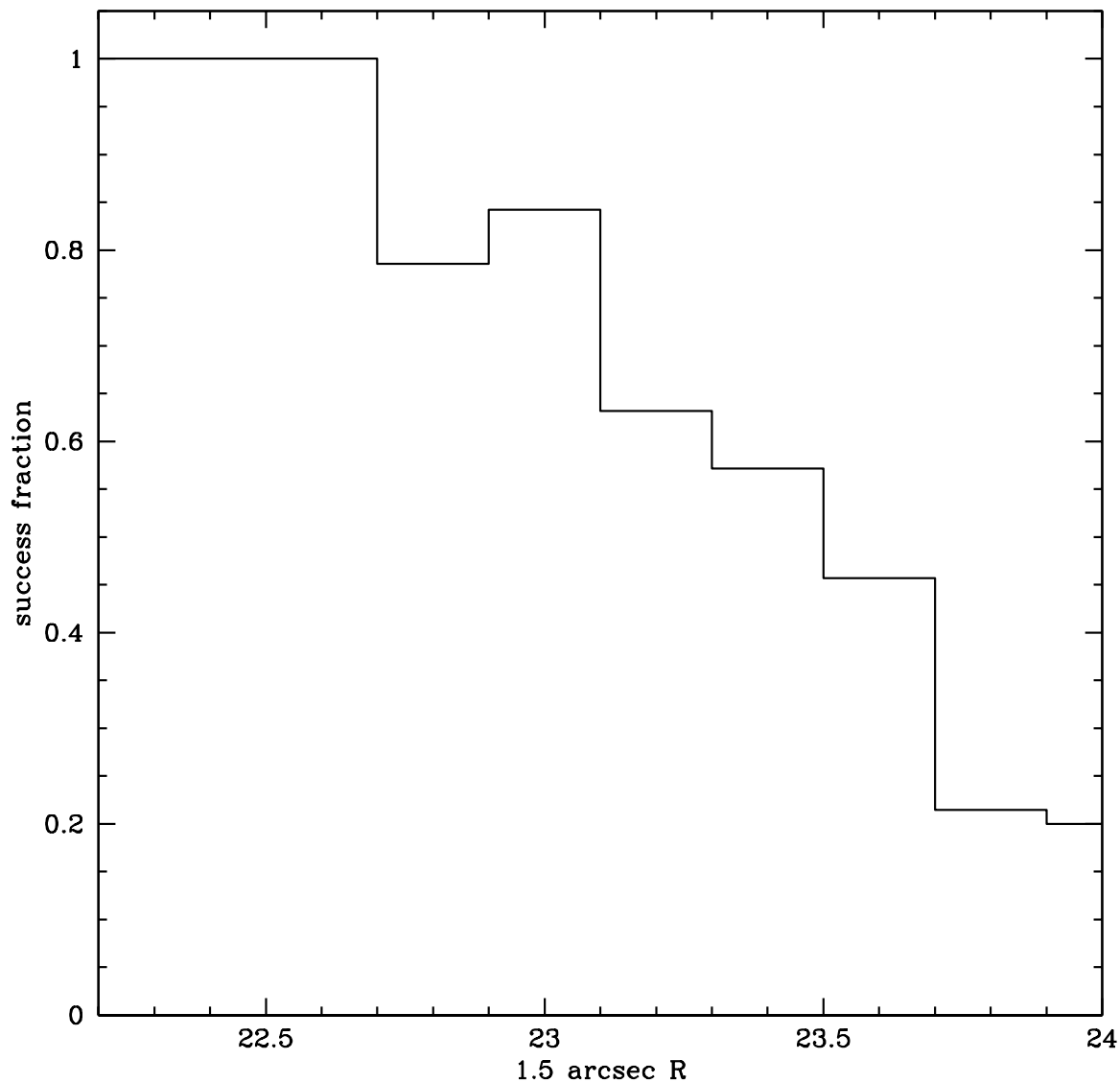


Fig. 22.— The fraction of objects which have successful redshift measurements as a function of the light down the fiber, a 1.5'' aperture. All of the lowest central surface brightness objects with successful redshifts have strong emission lines.

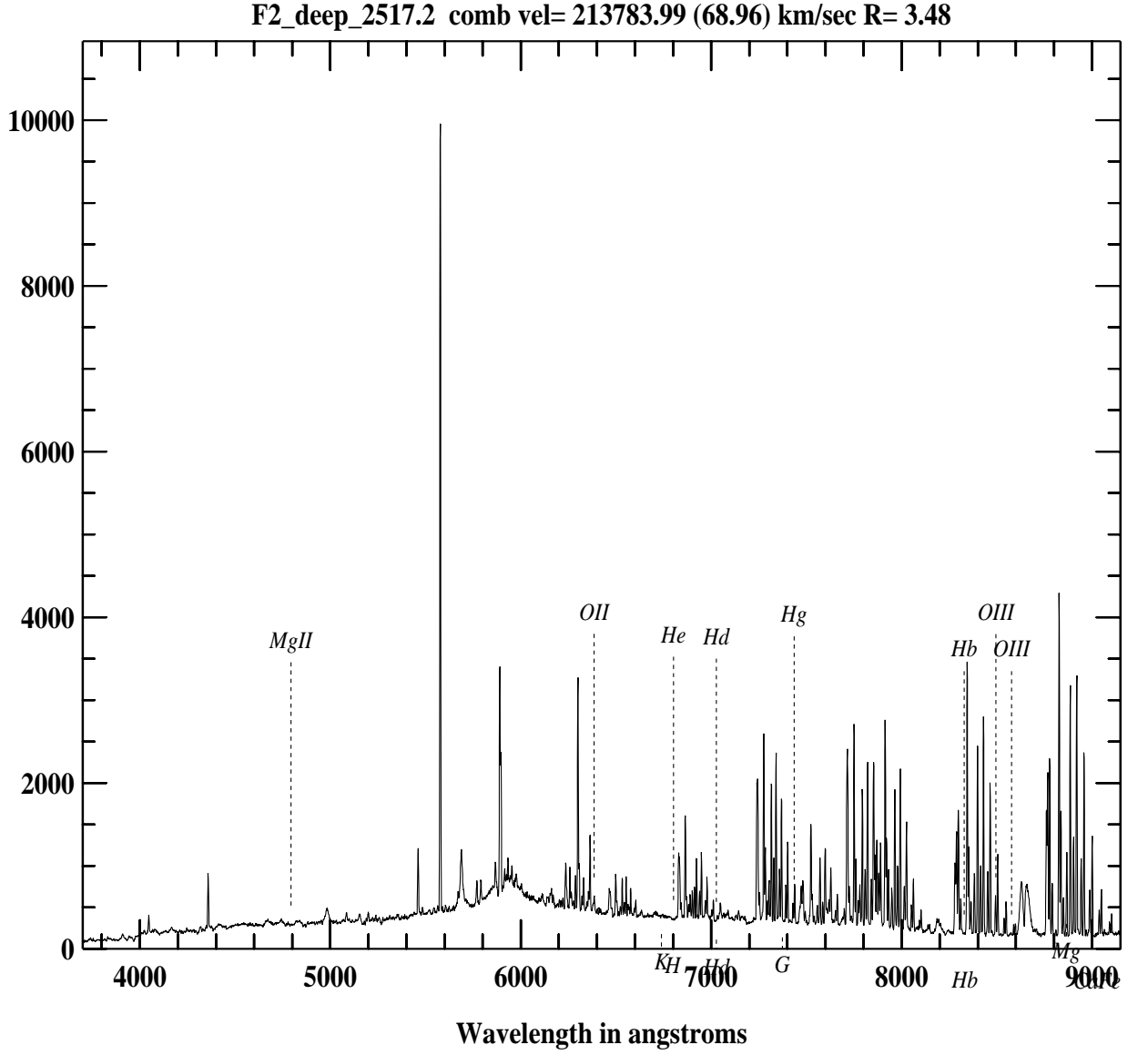


Fig. 23.— The spectrum of an $R=22.06$ galaxy with a reliable absorption line redshift of 0.71, before sky subtraction.

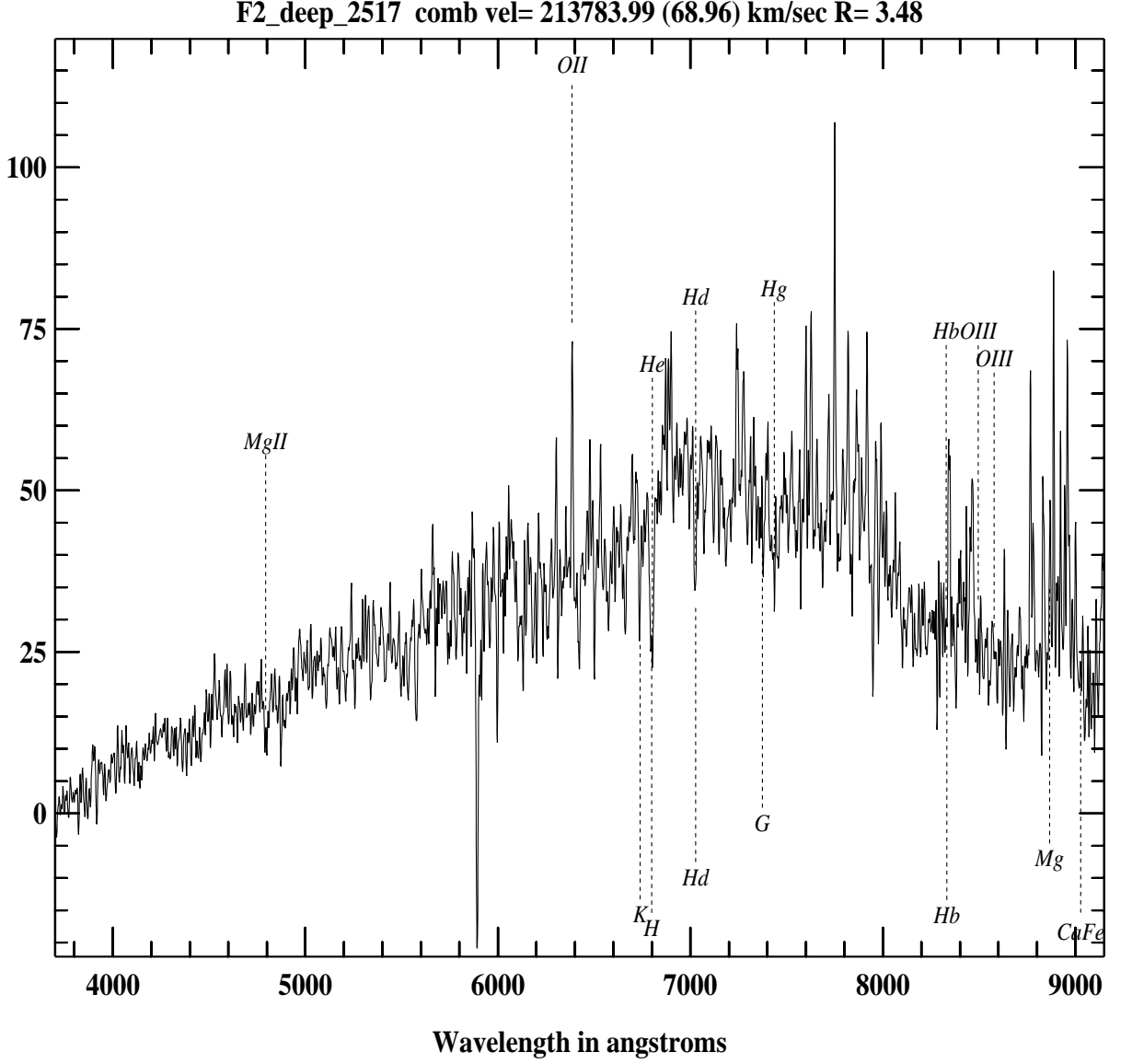


Fig. 24.— The spectrum of an $R=22.06$ galaxy with a reliable absorption line redshift of 0.71, after sky subtraction. The $1.5''$ diameter aperture magnitude is 22.97. The sky subtraction (see text) is effectively limited by Poisson noise.

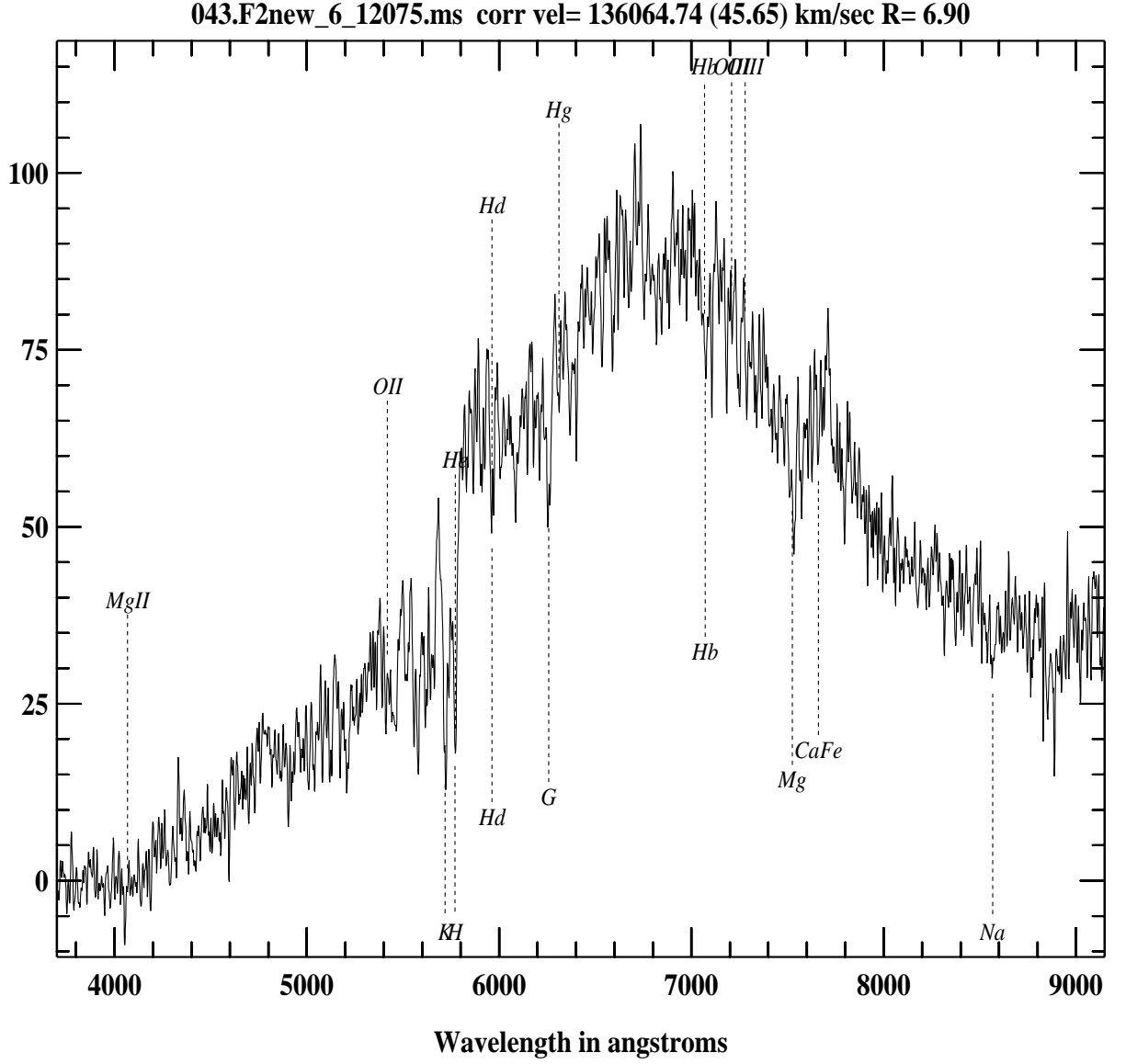


Fig. 25.— The spectrum of a typical absorption line galaxy, from a one hour exposure with the moon up. The object has an isophotal R magnitude of 19.00, a $1.5''$ magnitude of 21.23, and a redshift of 0.45.

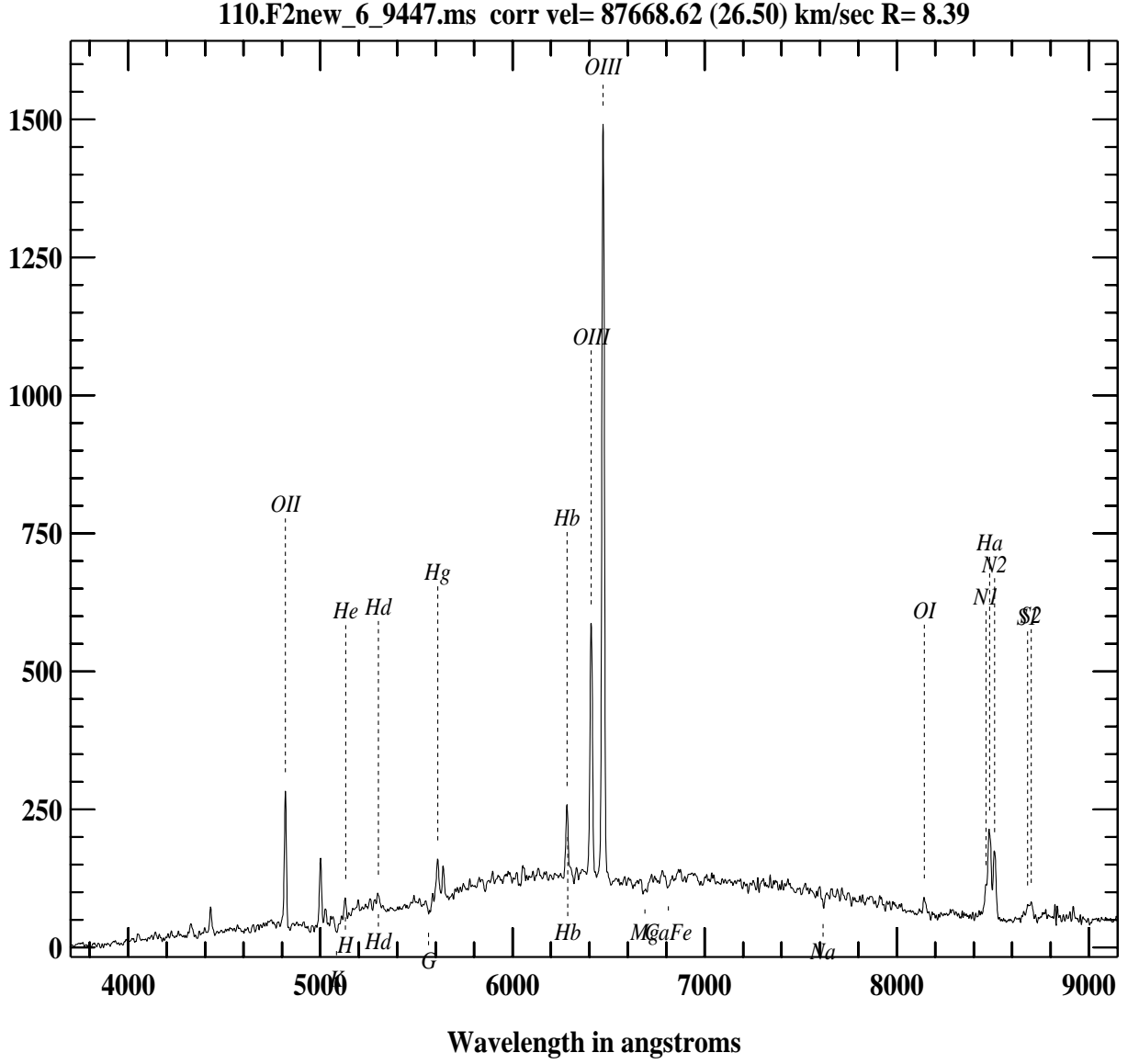


Fig. 26.— The spectrum of a typical emission line galaxy, from a one hour exposure with the moon up. The object has an isophotal R magnitude of 19.12, a $1.5''$ magnitude of 20.31, and a redshift of 0.29.

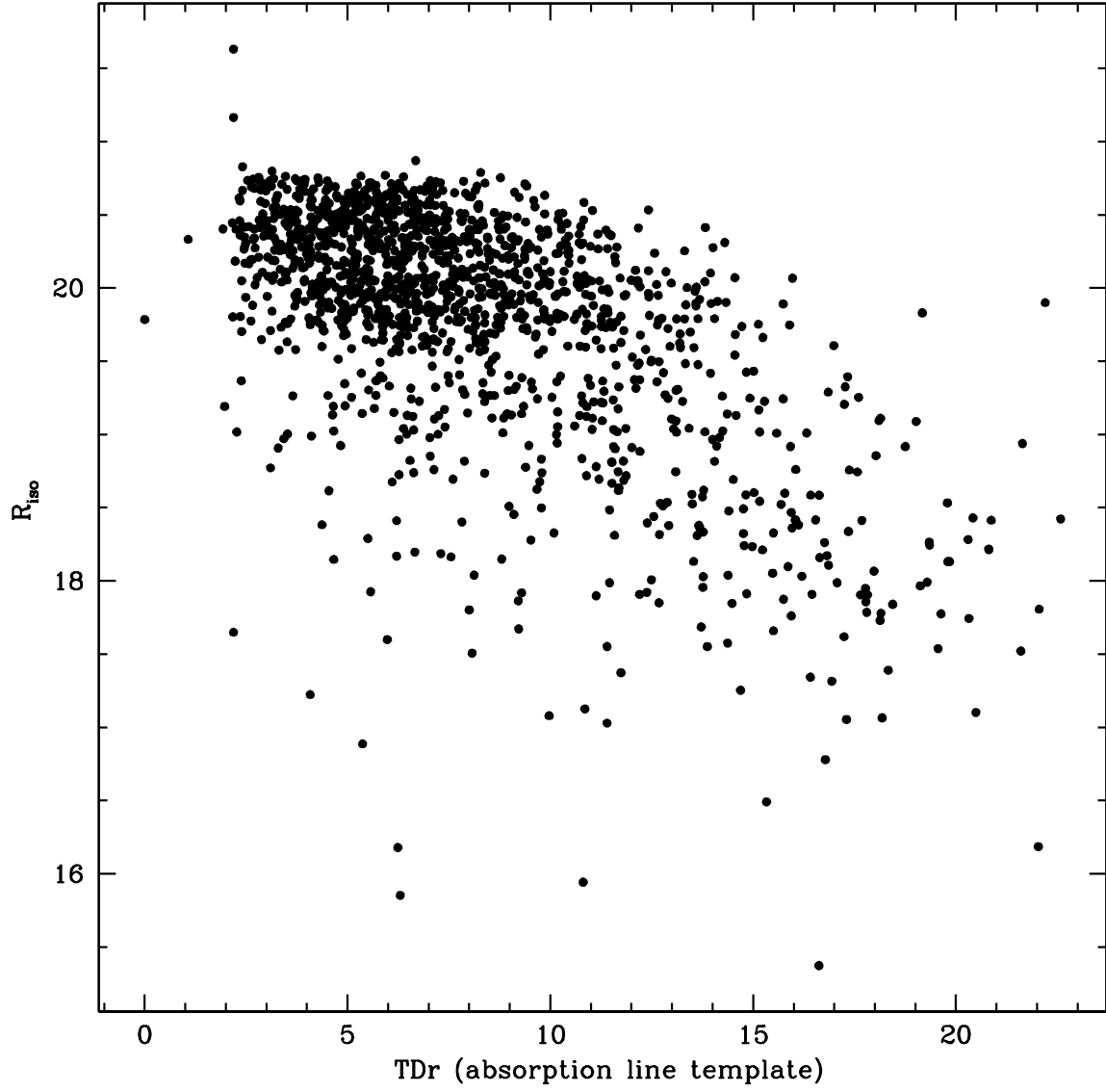


Fig. 27.— The isophotal R magnitude vs. the quality of the redshift as measured by the Tonry & Davis (1979) r statistic for 1455 one hour exposures of absorption line galaxies.

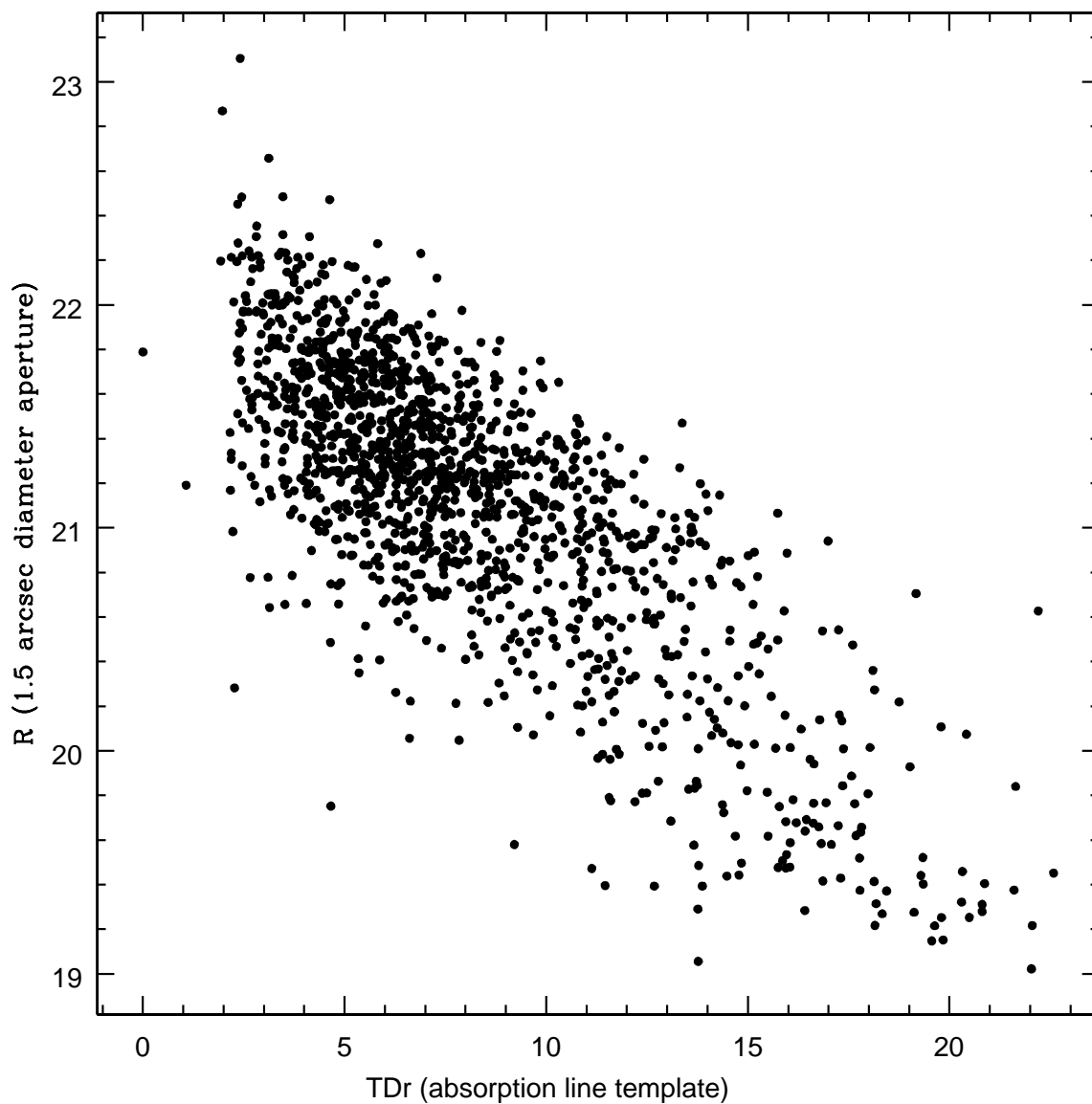


Fig. 28.— The $1.5''$ aperture R magnitude vs. the quality of the redshift as measured by the Tonry & Davis (1979) r statistic for 1455 one hour exposures of absorption line galaxies.

Table 1. Fiber Positioner Move Times

Move Parameter	X & Y Axes	Z Axis	Θ & Φ Axes	Gripper
S-Curve Time	0.030 s	0.015 s	0.020 s	0.003 s
Acceleration Time	0.100 s	0.030 s	0.070 s	0.050 s
Velocity	700 mm s ⁻¹	120 mm s ⁻¹	7 mm s ⁻¹	938 steps s ⁻¹
Settling Time ^a	0.100 s	0.050 s	0.100 s	0 s
Typical Move	150 mm	10 mm	2 mm	38 steps
Typical Move Time ^b	0.467 s ^c	0.193 s	0.426 s ^c	0.040 s

^aTime for servo system to reach position error less than 0.005 mm.

^bWe ignore the small motion during the S-curve acceleration, so these times are a slight overestimate.

^cThe XY and $\Theta\Phi$ moves are executed simultaneously, so the longer time will dominate.

Table 2. Fiber Positioning Error Sources

Error Source	Error Magnitude (mm)
Servo Loop Closure	0.005
Axis Calibration onto Orthogonal Cartesian Coordinates	0.008
Button Release Error	0.008
Calibration of Fiber Within Button	0.005
Focal Surface Flexure Correction	0.005 ^a
Flexure of Guide Probes During Observation	0.005 ^a
Total Positioning Error Added in Quadrature	0.015
Total Positioning Error Summed	0.036

^aEstimated

Table 3. Fiber Positioning Reconfiguration Overhead

Activity	Elapsed Time (s)
Readout CCD and Request Slew	60 s
Slew Telescope to Zenith	60 s
Reconfigure Fibers	320 s
Move Guider Probes	30 s
Slew to WFS Star	60 s
Acquire WFS and Correct	300 s
Slew to Field and Track	30 s
Setup on Guide Stars	180 s
Total	1040 s

^aEstimated